1
2
3
4
5
6
7
8
9
10
11

Systemic muscle wasting and coordinated tumour response drive tumourigenesis

Holly Newton[1], Yi-Fang Wang[1], Laura Camplese[1], André E.X. Brown[1,2]
and Susumu Hirabayashi[1,2]*

[1] Medical Research Council (MRC) London Institute of Medical Sciences (LMS),
Du Cane Road, London W12 0NN, United Kingdom
[2] Institute of Clinical Sciences (ICS), Faculty of Medicine, Imperial College London,
Du Cane Road, London W12 0NN, United Kingdom
* Correspondence: susumu.hirabayashi@lms.mrc.ac.uk

SUMMARY

Cancer cells demand excess nutrients to support their proliferation, but how tumours exploit extracellular amino acids during systemic metabolic pertubations remain incompletely understood. Here we use a *Drosophila* model of obesity-enhanced tumourigenesis to uncover a systemic host-tumour nutrient circuit that supports tumour growth. We demonstrate coordinate induction of systemic cachexia-like muscle wasting with tumour-autonomous SLC36-family amino acid transporter expression as a proline-scavenging programme to drive tumourigenesis. This coordinated induction of cachexia and SLC36-transporters pertains to human kidney cancer and associates with significantly worse survival outcomes. We identify Indole-3-propionic acid as an optimal amino acid derivative to rationally target the proline-dependency of tumour growth. Combining insights from whole-animal *Drosophila* models and human cancer database analysis provides a powerful approach towards the identification and therapeutic exploitation of the amino acid vulnerabilities of tumourigenesis in the context of perturbed systemic metabolic network.

40   Cancer cells require a constant supply of metabolic intermediates to support their proliferation.
41   To meet the biosynthetic demands associated with tumourigenesis, cancer cells actively acquire
42   nutrients from the extracellular space[1-5]. Cancer is a systemic disease that associates with a range
43   of host metabolic abnormalities such as obesity, insulin resistance, and cancer-associated
44   cachexia; each of which alter the host systemic nutritional environment. These changes in both
45   nutrient composition and availability may have profound effects on cancer development and
46   progression. However, how cancer cells sense and respond to nutritional changes in the context
47   of organismal metabolic alterations remains an under-explored area in cancer biology.

48   Cancer-associated cachexia is a systemic metabolic syndrome of weight loss associated
49   with progressive skeletal muscle wasting[6,7]. The multifactorial and heterogeneous condition of
50   cachexia involves a complex multi-organ interplay, which has impeded its comprehensive
51   understanding at the molecular level[8]. It remains an intriguing open question in the field as to
52   whether cancer-associated cachexia is an innocent bystander, or an active metabolic programme
53   designed to meet the nutrient demands of tumourigenesis. Here we leverage a *Drosophila* model
54   of obesity-enhanced tumourigenesis to directly address this question in the whole-animal setting.
55   We demonstrate that obesity-enhanced tumours require proline for their growth, and that
56   tumours induce systemic muscle wasting and SLC36-family transporter expression as a
57   coordinated mechanism to exploit exogenous proline for tumourigenesis. We link these
58   mechanistic insights from our fly study with human cancer data, to rationally target the proline-
59   dependency of tumours as an approach to suppress tumour growth in the context of perturbed
60   systemic metabolic network.

Obesity-enhanced tumours induce muscle wasting

62   We previously reported a *Drosophila* larval model to study the systemic effects of diet-induced
63   obesity and insulin resistance on tumour progression[9,10]. Feeding *Drosophila* larvae a high-
64   sucrose diet (HSD) led to sugar-dependent metabolic defects including accumulation of fat,
65   systemic insulin resistance, and hyperglycemia[11]. Targeted co-activation of Ras- and Src-
66   pathways—by expression of an oncogenic isoform of *dRas1, ras1^{G12V}* and knockout of the
67   negative regulator of Src, C-terminal src kinase (*csk^{-/-}*)—in the *Drosophila* eye epithelia led to
68   the development of benign tumours in animals raised on a control diet (CD) (Fig. 1a).
69   Comparatively, feeding *ras1^{G12V};csk^{-/-}* animals a HSD promoted aggressive tumour growth in
70   the eye epithelia (Fig. 1b), associated with secondary tumour formation (Fig. 1b, arrowheads),
71   and led to larval lethality (Fig. 1c).

72   To explore the interplay between diet-induced obesity, tumour progression, and systemic
73   organ wasting, we assessed the peripheral tissues of *ras1^{G12V};csk^{-/-}* animals—including the larval
74   fat body and body wall skeletal muscle. Fat body lipid accumulation was elevated under HSD
75   feeding, as assessed by the neutral lipid stain Nile Red (Fig. 1d, e). Strikingly, despite possessing
76   an intact fat body, *ras1^{G12V};csk^{-/-}* animals raised on HSD exhibited significant skeletal muscle
77   wasting as visualised by F-actin and myosin staining (Fig. 1f, g). To quantify the severity of
78   muscle wasting—as assessed by imaging the fourth abdominal segment of the larval body wall
79   muscle (Extended Data Fig. 1a)—we scored animals into one of four categories: none, minor,
80   moderate or strong wasting (Extended Data Fig. 1b-e). While most (83.33%) of the *ras1^{G12V};csk^{-/-}*
81   animals raised on a CD displayed intact skeletal muscle, 100% of animals raised on a HSD
82   exhibited muscle wasting of some degree (Fig. 1h). Muscle wasting was progressive; intact
83   skeletal muscle was observed at the earlier stages of larval development, and as diet-enhanced
84   tumourigenesis proceeded, skeletal muscle wasting increased (Extended Data Fig. 1f-j).
85   Functional locomotion defects—as measured by video tracking analysis[12,13]—were observed in
86   *ras1^{G12V};csk^{-/-}* animals raised on a HSD (Fig. 1i). Significant defects were observed in average
87   speed, body curvature and body posture (Fig. 1j-l).

88   HSD feeding in *ras1^{G12V};csk^{-/-}* animals led to a developmental delay in reaching the third
89   instar larval stage[9]. To rule out the possibility that observed muscle wasting was due to an
90   extended larval period, we ablated the prothoracic gland (PG)—an ecdysteroid-producing
91   organ—using the PG-specific *phantom (phm)-GAL4* driver to suppress pupariation. PG-ablated
92   larvae, that were raised on a HSD and chronologically age-matched (day 6 after PG-ablation) to
93   *ras1^{G12V};csk^{-/-}* animals in HSD, exhibited minimal muscle wasting in a HSD (Extended Data Fig.
94   2a-c). Together these results indicate that extended larval period alone is insufficient to account
95   for the muscle wasting observed in *ras1^{G12V};csk^{-/-}* animals in HSD, and instead support a specific
96   role for diet-enhanced tumourigenesis in promoting muscle wasting.

Muscle wasting releases amino acids

98   A consequence of skeletal muscle wasting is protein degradation and subsequent release of free
99   amino acids into the circulation. We performed a genome-wide transcriptional profiling analysis
100   of dissected body-wall muscle from *ras1^{G12V};csk^{-/-}* animals raised on CD and HSD, from early
101   through to late stages of muscle wasting (Extended Data Fig. 3a). As expected, Gene Set
102   Enrichment Analysis (GSEA) revealed a progressive deregulation of muscle structure
103   organisation in *ras1^{G12V};csk^{-/-}* animals in HSD (Extended Data Fig. 3b). A previous report
104   demonstrated that ubiquitin-proteasome system (UPS) deregulation promotes skeletal protein
105   degradation and muscle wasting via induction of the unfolded protein response (UPR)[14].
106   Consistent with this report, GSEA from muscle RNA-sequencing data revealed aberrant UPS
107   function (Extended Data Fig. 3c) which correlated with accumulation of poly-ubiquitinated
108   proteins (Extended Data Fig. 3d, e). This was coupled with an increase in UPR (Extended Data
109   Fig. 3f), as visualised by increased perinuclear staining of the UPR-marker GRP-78[15] (Extended
110   Data Fig. 3g, h).

111   Through targeted metabolomic analysis, we measured an increase in circulating levels of
112   amino acids in the hemolymph of *ras1^{G12V};csk^{-/-}* animals raised on a HSD relative to CD (Fig.
113   2a and Extended Data Fig. 4a, b). Together with increased circulating 3-methylhistidine, a
114   biomarker for muscle atrophy[16] (Extended Data Fig. 4c), these results indicate that muscle
115   protein degradation takes place in *ras1^{G12V};csk^{-/-}* animals raised on a HSD. Since amino acids are
116   one of the largest contributors to increased cell mass in proliferating cells[1], our observations
117   suggested muscle wasting as a source of circulating amino acids for tumour progression.

Proline transporters are required for tumour growth

119   To explore candidates that could be responsible for tumour-specific amino acid utilisation, we
120   focused on amino acid transporters. Through RNA-sequencing analysis of tumour tissue from
121   *ras1^{G12V};csk^{-/-}* animals raised on CD and HSD, we characterised the expression profile of amino
122   acid transporters across the SLC1, SLC7, SLC36 and SLC38 families (Extended Data Fig. 5a,
123   5b). Subsequent qPCR validation confirmed that amino acid transporters of the SLC7 family
124   (*minidiscs (mnd), JhI-21* and CG5535) and SLC36-family (*CG8785, pathetic (path)*, and
125   *CG1139*) were upregulated in tumours of *ras1^{G12V};csk^{-/-}* animals raised on a HSD compared to
126   CD (Fig. 2b). Of note, expression levels of *Slimfast (slif)*—another SLC7-family member and an
127   amino acid transporter previously implicated in tumour-specific usage of amino acids[17,18]—was
128   downregulated in Ras/Src-tumours in HSD (Fig. 2b).

129   Reducing expression of *mnd (ras1^{G12V};csk^{-/-},mnd^{RNAi}), JhI-21 (ras1^{G12V};csk^{-/-},JhI-21^{RNAi}),*
130   *CG5535 (ras1^{G12V};csk^{-/-},CG5535^{RNAi}), slif (ras1^{G12V};csk^{-/-},slif^{RNAi})* or *CG8785 (ras1^{G12V};csk^{-/-},*
131   *CG8785^{RNAi})*, had no effect on primary tumour size (Fig. 2c-h). Strikingly, reducing expression
132   of *path (ras1^{G12V},path^{RNAi};csk^{-/-})* or CG1139 (*ras1^{G12V};csk^{-/-},CG1139^{RNAi}*) almost completely
133   suppressed diet-mediated Ras/Src-tumour growth (Fig. 2i, j and Extended Data Fig. 5c, d).
134   Importantly, reduction in *path* or *CG1139* levels had minimal effect on tumour growth in

135   *ras1^{G12V};csk$^{-/-}$* animals fed a CD (Fig. 2k-m) indicating that neither are required for benign
136   tumour growth. Altogether, these results demonstrate that Path and CG1139 are specifically
137   required for diet-mediated enhancement of Ras/Src-tumour growth.

138   We confirmed elevation of Path and CG1139 protein levels in Ras/Src-tumours in HSD
139   using the Path- and CG1139-specific antibodies[19] (Fig. 2n, o, q, r, and Extended Data Fig. 5e, f).
140   *Path* has been previously identified as one of the growth-regulatory factors under control of the
141   Hippo signalling pathway downstream transcriptional co-activator Yki[20]. Over-expression of
142   Warts (Wts)—and therefore inhibition of Yki-activity—in Ras/Src-activated cells (*ras1^{G12V};csk$^{-/-}$,wts*)
143   led to decreased Path protein but not CG1139 levels in animals fed a HSD (Fig. 2p, s).
144   While Path was elevated specifically in Ras/Src-activated tumours in HSD (Fig. 2n, o, and
145   Extended Data Fig. 5e), the elevation of CG1139 was not specific to tumours but was rather
146   dependent on high sugar diet (Fig. 2q, r, and Extended Data Fig. 5f). Together with our previous
147   study demonstrating that diet-enhanced Ras/Src-tumours activate Yki[10], we conclude that the
148   Hippo signalling downstream effector Yki mediates *path* expression in *ras1^{G12V};csk$^{-/-}$* animals
149   raised on a HSD.

Proline promotes tumour growth via Path

151   Mammalian SLC36-family amino acid transporters including SLC36A1 and SLC36A2 transport
152   alanine, glycine and proline[21]. Proline was the most highly increased amino acid in the
153   hemolymph of *ras1^{G12V};csk$^{-/-}$* animals in HSD (Fig. 2a and Extended Data Fig. 4b). Over-
154   expression of Path (*ras1^{G12V};csk$^{-/-}$,pathA*) or CG1139 (*ras1^{G12V},CG1139;csk$^{-/-}$*) had a negligible
155   effect on tumour growth in Ras/Src-activated cells on CD, indicating that transporter expression
156   alone is insufficient to promote tumourigenesis (Fig. 3a-c).

157   To mimic the elevation of circulating proline levels under conditions of muscle wasting,
158   we carried out dietary supplementation of proline. Feeding animals CD supplemented with 100
159   mM L-proline had minimal effect on tumour growth of *ras1^{G12V};csk$^{-/-}$* animals in CD (Fig. 3d).
160   Intriguingly however, feeding proline in *ras1^{G12V};csk$^{-/-}$,pathA* animals strongly promoted tumour
161   growth in CD (Fig. 3e). In striking contrast, proline feeding in *ras1^{G12V},CG1139;csk$^{-/-}$* animals
162   had no effect on tumour growth (Fig. 3f). Of note, feeding proline in animals with path- or
163   CG1139-overexpressing clones had minimal effect on tissue growth (Fig. 3g-i), suggesting that
164   proline-Path mediated enhancement of tissue growth requires an oncogenic background.
165   Altogether, these results indicate that coordinated elevation of systemic proline availability and
166   tumour-autonomous transporter expression is required to promote Ras/Src-tumour growth.

167   Feeding excess L-glycine or L-alanine had minimal growth promoting effect in
168   *ras1^{G12V};csk$^{-/-}$* and *ras1^{G12V};csk$^{-/-}$,pathA* animals (Fig. 3j, k, m, n). Similarly, feeding the
169   biologically inert isomer of proline—D-proline—had no effect on tumour growth in both
170   *ras1^{G12V};csk$^{-/-}$* and *ras1^{G12V};csk$^{-/-}$,pathA* animals (Fig. 3l, o), thereby indicating that tumour
171   response is specific to L-proline. Altogether, our data highlight the proline vulnerability of
172   obesity-enhanced Ras/Src-tumours and uncover modulation of amino acid transporter repertoire
173   as a strategy to meet the nutrient requirements of tumourigenesis.

Muscle wasting affects tumour growth

175   Our results suggest that cachexia-like muscle wasting and associated circulating proline
176   availability promote Ras/Src-tumourigenesis. Therefore, targeting tumour-derived factors which
177   mediate muscle wasting may not only attenuate muscle wasting but also suppress tumour growth.
178   To explore this concept, we set out to identify tumour-derived factors which mediate muscle
179   wasting. Through genome-wide transcriptional profiling analysis of dissected tumour tissue from
180   *ras1^{G12V};csk$^{-/-}$* animals raised on CD and HSD (Extended Data Fig. 5a), we identified *branchless*
181   (*bnl*), a *Drosophila* fibroblast growth factor (FGF) ligand as one of the most highly upregulated

4

182 secreted factors in $ras1^{G12V};csk^{-/-}$ tumours in animals raised on a HSD (upregulated 5.02-
183 log2fold)(Fig. 4a and Extended Data Fig. 6a). Among the three known *Drosophila* FGF ligands
184 (Bnl, Pyramus, and Thisbe), *bnl* was the only FGF ligand to be highly elevated in
185 $ras1^{G12V};csk^{-/-}$ tumours in HSD (Fig. 4a). Consistently, Bnl protein expression was strongly
186 upregulated in $ras1^{G12V};csk^{-/-}$ tumours of animals fed a HSD (Fig. 4b, c).

187 Reducing *bnl* expression in Ras/Src-activated tumours ($ras1^{G12V};csk^{-/-},bnl^{RNAi}$) attenuated
188 muscle wasting in animals raised on a HSD (Fig. 4g-i and Extended Data Fig. 6f, k), indicating
189 that tumour-derived Bnl is required for muscle wasting. Tumour-derived factors recently
190 implicated in cachexia-like organ wasting include ImpL2 and Pvf1[22-24]. These were also elevated
191 both transcriptionally and at the protein level in $ras1^{G12V};csk^{-/-}$ tumours in HSD (Extended Data
192 Fig. 6a-e). However, reducing the levels of either ImpL2 ($ras1^{G12V};csk^{-/-},ImpL2^{RNAi}$) or Pvf1
193 ($ras1^{G12V},pvf1^{RNAi};csk^{-/-}$) failed to rescue muscle wasting as efficiently as *bnl* in our diet-enhanced
194 Ras/Src-tumour model (Extended Data Fig. 6g, h, k). Altogether, these results establish Bnl as a
195 functionally relevant tumour-secreted factor that contributes to muscle wasting in animals with
196 diet-enhanced Ras/Src-tumours.

197 Importantly, reducing *bnl* expression in diet-enhanced Ras/Src- tumours ($ras1^{G12V};csk^{-/-}$
198 $,bnl^{RNAi}$) not only attenuated systemic muscle wasting but also suppressed tumour growth and
199 larval lethality (Fig. 4d-f and Extended Data Fig. 6f). Tumour autonomous Bnl and its receptor
200 Breathless (Btl) signalling has been implicated in tumourigenesis[25]. However, reducing the
201 levels of *btl* in Ras/Src-activated tumours ($ras1^{G12V},btl^{RNAi};csk^{-/-}$) had minimal effect on primary
202 tumour size or muscle wasting, indicating that tumour autonomous reduction of Bnl-Btl
203 signalling was not responsible for suppression of tumour growth in $ras1^{G12V};csk^{-/-},bnl^{RNAi}$
204 animals (Extended Data Fig. 6i-k). Together, these results reveal that systemic muscle wasting
205 has a functional effect on tumour growth.

206 We next examined the link between proline-mediated Ras/Src tumour growth and Bnl-
207 mediated muscle wasting. Feeding proline in $ras1^{G12V};csk^{-/-},pathA$ animals not only promoted
208 tumour growth (Fig. 3e), but also led to elevated tumour expression of Bnl (Extended Data Fig.
209 7a, b) and subsequent muscle wasting (Extended Data Fig. 7c-e). Together this demonstrates that
210 Path-dependent proline-enhancement of tumour growth promotes Bnl-mediated muscle wasting.
211 Overall, this data implicates the coordinate induction of amino acid transporter expression,
212 coupled with cachexia-like muscle wasting, as sufficient to establish a feed-forward host-tumour
213 circuit to drive tumour growth.

214 **Translation to human cancer**

215 To examine whether coordinated induction of cachexia and amino acid transporter expression
216 pertains to human cancers, we examined the transcriptional profile of tumour samples from
217 patients in The Cancer Genome Atlas (TCGA), across a panel of cancer types[26]. As with most
218 databases, patient data is not annotated for the presence or absence of cachexia, however an
219 earlier study adopted the expression of cachectic factors—IL-1A, IL-1B, IL-6, IL-8 and TNF-
220 α—as a proxy for cachexia (Cachexia Score)[27]. In humans, the SLC36 family of amino acid
221 transporters consists of four members: SLC36A1-A4. We focused our analysis on SLC36A1 and
222 SLC36A4; the A2 and A3 isoforms were excluded due to their low tumour expression levels.
223 From the six cancer types analysed, Cachexia Score correlated positively with both SLC36A1
224 and SLC36A4 expression in kidney cancer, SLC36A1 expression in pancreatic cancer, and
225 SLC36A4 expression in liver cancer patients (Fig. 5a-e). To determine whether coordinated
226 induction of cachectic factors and SLC36-family transporters affected prognosis, we compared
227 survival outcomes in patient groups with high and low expression of cachectic factors and SLC36
228 transporters. Strikingly, kidney cancer patients with both a high Cachexia Score and high SLC36
229 transporter expression had significantly worse survival compared with those exhibiting both a

low Cachexia Score and low SLC36 transporter expression (Fig. 5f, g). Similarly patients with both a high Cachexia Score and a high SLC36A1 expression in pancreatic cancer or a high Cachexia Score and a high SLC36A4 expression in liver cancer exhibited worse survival rates, albeit not reaching statistical significance (Fig. 5h, i). Overall, our data demonstrates that coordinated induction of cachectic factors and SLC36 transporter expression has a strong negative effect on patient survival in human kidney cancer.

Targeting proline vulnerability of tumours

Taken together, our *Drosophila* data and human cancer database analysis specifically highlight SLC36-family transporters as a target for therapeutic intervention in tumours with proline vulnerability. A previous *in vitro* study using a human cancer cell line explored amino acid- and amino acid derivative-specificities of SLC36A1[28]. By selecting competitive, non-transported inhibitors of SLC36A1 from this study, we performed a whole-animal *Drosophila* screen to identify candidates that suppress tumour growth and display minimal whole-animal toxicity. Feeding *ras1^{G12V};csk$^{-/-}$* animals a HSD supplemented with 5-Hydroxy-L-tryptophan led to animal lethality at the early larval stages, indicative of whole-animal toxicity. Feeding *ras1^{G12V};csk$^{-/-}$* animals a HSD supplemented with either L-tryptophan or Indole-5-carboxylic acid led to successful larval development, but had no inhibitory effect on tumour growth (Figure 6a-c). However, feeding *ras1^{G12V};csk$^{-/-}$* animals a HSD supplemented with Indole-3-propionic acid (IPA) dramatically suppressed tumour growth in HSD (Fig. 6d). Strikingly, 66.2% of IPA-fed *ras1^{G12V};csk$^{-/-}$* animals achieved pupariation in HSD, revealing significant tumour-suppressing efficacy coupled with minimal whole-animal toxicity (Fig. 6g-i). Furthermore, IPA feeding had no effect on benign tumour growth in *ras1^{G12V};csk$^{-/-}$* animals raised on CD (Fig. 6e, f), supporting the notion that SLC36 inhibition only limits the growth of tumours with proline vulnerability.

DISCUSSION

Our study reveals a systemic amino acid-utilising circuit whereby obesity-enhanced tumours induce muscle wasting as a systemic metabolic network to drive tumourigenesis. A consequence of muscle wasting in *ras1^{G12V};csk$^{-/-}$* animals raised on HSD was increased release of proline into the circulation (Fig. 2a). Plasma amino acid profiling of patients with sarcopenia—a condition of muscle wasting associated with aging—showed elevated plasma proline levels[29], indicating that elevated free circulating proline is a common feature of muscle wasting. We identify a proline vulnerability of obesity-enhanced tumours; SLC36-family proline transporter Path is required for tumour growth and exogenous proline promotes tumourigenesis through Path (Fig. 2, 3). We highlight two layers of coordination in tumour metabolic response: (i) at the whole organism level - by promoting cachexia-like muscle wasting and systemic amino acid availability, and (ii) at the tumour-autonomous level - by altering amino acid transporter repertoire (Fig. 6j).

The insights obtained from our *Drosophila* model were sufficient to predict altered cancer patient outcomes. Human cancer database analysis demonstrates that co-expression of cachectic factors alongside both SLC36A1 and SLC36A4 amino acid transporters correlates with significantly worse patient survival in kidney cancer patients (Fig. 5). Proline has been shown to be a limiting amino acid for protein synthesis in kidney cancers[30]. Therefore, reducing proline uptake with SLC36-inhibitors—as exemplified here by use of Indole-3-propionic acid (Fig. 6)—may warrant consideration as a therapeutic strategy to break the nutritional circuit between cachexia-like muscle wasting and tumour growth in human kidney cancer patients.

METHODS

Fly stocks. *UAS-ras1^{G12V}*, *UAS-lacZ*, *UAS-bnl$^{RNAi/TRiP}$*, *UAS-path$^{RNAi/TRiP}$* and *UAS-wts* flies were obtained from the Bloomington *Drosophila* Stock Center. *UAS-bnl$^{RNAi/GD}$*, *UAS-path$^{RNAi/KK}$*, *UAS-Pvf1$^{RNAi/GD}$*, *UAS-mnd$^{RNAi/GD}$*, *UAS-slif$^{RNAi/GD}$*, *UAS-JhI-21$^{RNAi/GD}$*, *UAS-ImpL2$^{RNAi/GD}$*, *UAS-CG8785$^{RNAi/GD}$*, *UAS-CG5535$^{RNAi/GD}$*, *UAS-CG1139$^{RNAi/GD}$*, *UAS-CG1139$^{RNAi/KK}$*, *UAS-btl$^{RNAi/GD}$* and *UAS-btl$^{RNAi/KK}$* flies were obtained from the Vienna *Drosophila* Resource Center.

The following stocks were kindly provided to us: *FRT82B, csk^{Q156Stop}* by A. O'Reilly and M. Simon; *ey(3.5)-FLP1* by G. Halder; *Phm-gal4; tub-gal80^{ts}* and *UAS-grim* by T. Koyama; *UAS-pathA/TM6B* by J. Parrish; *UAS-CG1139* by D. Goberdhan.

To create eyeless-driven GFP-labeled clones, the MARCM system was used. Flies with the genotype *ey(3.5)-FLP1; act > y+ > gal4,UAS-GFP; FRT82B, tub-gal80* were crossed to flies with the following genotypes: (1) *UAS-ras1^{G12V}*; *FRT82B, csk^{Q156Stop}/TM6b*; (2) *UAS-ras1^{G12V}*; *FRT82B, csk^{Q156Stop}, UAS-mnd$^{RNAi/GD}$/TM6b*; (3) *UAS-ras1^{G12V}*; *FRT82B, csk^{Q156Stop}, UAS-JhI-21$^{RNAi/GD}$/TM6b*; (4) *UAS-ras1^{G12V}*; *FRT82B, csk^{Q156Stop}, UAS-CG5535$^{RNAi/GD}$/TM6b*; (5) *UAS-ras1^{G12V}*; *FRT82B, csk^{Q156Stop}, UAS-slif$^{RNAi/GD}$/TM6b*; (6) *UAS-ras1^{G12V}*; *FRT82B, csk^{Q156Stop}, UAS-CG8785$^{RNAi/GD}$/TM6b*; (7) *UAS-ras1^{G12V}, UAS-path$^{RNAi/KK}$*; *FRT82B, csk^{Q156Stop}/TM6b*; (8) *UAS-ras1^{G12V}*; *FRT82B, csk^{Q156Stop}, UAS-CG1139$^{RNAi/GD}$/TM6b*; (9) *UAS-ras1^{G12V}, UAS-path$^{RNAi/TRiP}$*; *FRT82B, csk^{Q156Stop}/TM6b*; (10) *UAS-ras1^{G12V}, CG1139$^{RNAi/KK}$*; *FRT82B, csk^{Q156Stop}/TM6b*; (11) *UAS-ras1^{G12V}*; *FRT82B, csk^{Q156Stop}, UAS-wts*; (12) *UAS-ras1^{G12V}*; *FRT82B, csk^{Q156Stop}, UAS-PathA/TM6b*; (13) *UAS-CG1139, UAS-ras1^{G12V}*; *FRT82B, csk^{Q156Stop}/TM6b*; (14) *UAS-lacZ; FRT82B*; (15) *FRT82B, UAS-PathA/TM6b*; (16) *UAS-CG1139; FRT82B*; (17) *UAS-ras1^{G12V}*; *FRT82B, csk^{Q156Stop}, UAS-bnl$^{RNAi/GD}$/SM6-TM6b*; (18) *UAS-ras1^{G12V}*; *FRT82B, csk^{Q156Stop}, UAS-bnl$^{RNAi/TRiP}$/TM6b*; (19) *UAS-ras1^{G12V}, UAS-btl$^{RNAi/GD}$*; *FRT82B, csk^{Q156Stop}/TM6b*; (20) *UAS-ras1^{G12V}, UAS-btl$^{RNAi/KK}$*; *FRT82B, csk^{Q156Stop}/TM6b*; (21) *UAS-ras1^{G12V}*; *FRT82B, csk^{Q156Stop}, UAS-ImpL2$^{RNAi/GD}$/TM6b*; (22) *UAS-ras1^{G12V}*; *FRT82B, csk^{Q156Stop}, UAS-Pvf1$^{RNAi/GD}$/TM6b*.

To carry out prothoracic gland ablation, *Phm-gal4; tub-gal80^{ts}/TM6b* flies were crossed with *UAS-grim* flies and reared at 18°C. At early third instar larval stage (day 12 in 18°C), cultures were switched to 29°C to inactivate *tub-gal80^{ts}*.

Cultures. Cultures were carried out on Bloomington semi-defined medium (https://bdsc.indiana.edu/information/recipes/germanfood.html) and contained sucrose (0.15 M and 1.0 M in CD and HSD, respectively) as the only purified sugar source. Ingredients were obtained from; Agar (Fisher Scientific; BP2641-1), Brewer's Yeast (MP Biomedicals; 903312, Lot: BCBN0171V), Yeast Extract (Sigma-Aldrich; 70161), Peptone (Sigma-Aldrich; 82303), Sucrose (Fisher Scientific; S/8560/63), Magnesium sulfate hexahydrate (Fluka; 00627), Calcium chloride dihydrate (Sigma-Aldrich; 223506), Propionic acid (Sigma-Aldrich; P1386), p-Hydroxy-benzoic acid methyl ester (Sigma-Aldrich; H5501). For dietary supplementation experiments, L-proline (Sigma-Aldrich; P5607), D-proline (Sigma-Aldrich; 858919), L-glycine (VWR Chemicals; 101196X) or L-alanine (Sigma-Aldrich; 7627) were added to CD to a final concentration of 100 mM. L-tryptophan (Sigma Aldrich; T0254), Indole-5-carboxylic acid (Sigma Aldrich; I5400) and Indole-3-propionic acid (Sigma Aldrich; 57400) were added to HSD and CD to a final concentration of 10 mM. Cultures were performed at 25°C unless otherwise noted. HSD feeding led to a developmental delay in reaching the third instar larval stage; all experiments were performed on late third instar larvae at day 8 after egg laying (CD) and day 14 after egg laying (HSD) unless otherwise noted.

326   **Immunohistochemistry.** Tissue was dissected in PBS, fixed in 4% PFA/PBS for 30' on ice,
327   washed in PBS-T, incubated with primary antibody in PAXDG (PBS containing 1% BSA, 0.3%
328   Triton X-100, 0.3% deoxycholate, and 5% goat serum), followed by washing and incubation
329   with secondary antibody in PAXDG and subsequent mounting in Vectashield with DAPI (Vector
330   Laboratories). Primary antibodies used were: rat anti-myosin (ab51098; Abcam; 1:100), mouse
331   anti-polyubiquitin (FK2; Enzo Life Sciences; 1:300), mouse anti-GRP-78 (E-4; Santa Cruz
332   Biotechnology; 1:50). Polyclonal Rabbit anti-CG1139 (1:200) was purified by New England
333   Peptide Inc., MA, USA. An amino acid sequence 26-40 was selected as the epitope. The
334   following primary antibodies were kindly gifted to us: rat anti-bnl (M. Krasnow; 1:50) guinea
335   pig anti-path (J. Parrish; 1:200), rat anti-ImpL2 (H. Stocker; 1:250), rat anti-pvf1 (B. Shilo;
336   1:200). Secondary antibodies used were: Alexa-488 and Alexa-568 conjugated anti-rat antibody
337   (Molecular Probes; 1:200), Alexa-488 and Alexa-568 conjugated anti-mouse antibody
338   (Molecular Probes; 1:200), Alexa-488 and Alexa-568 conjugated anti-rabbit antibody
339   (Molecular Probes; 1:200) and Alexa-568 conjugated anti-guinea pig antibody (Molecular
340   Probes; 1:200). TRITC-labelled rhodamine-phalloidin was used to visualise F-actin (R415;
341   Invitrogen; 1:500).
342
343   **Nile red staining.** Tissue was dissected in PBS, fixed in 4% PFA/PBS for 30' on ice, incubated
344   with 10 µg/mL Nile Red stain (N1142; ThermoFisher Scientific) in PBS for 30' on ice followed
345   by washing and subsequent mounting in Vectashield with DAPI.
346
347   **Muscle wasting quantification.** Individual larvae were washed and dissected in PBS. Larval
348   body wall muscle was stained with TRITC-labelled rhodamine-phalloidin (R415; Invitrogen;
349   1:500) to visualise F-actin. Individual animals were scored into categories each representing the
350   strength of muscle wasting from either "none"; "minor"; "moderate" or "strong" (Extended Data
351   Fig. 1a-e). Scores were assigned based on wasting of the ventral longitudinal, lateral oblique and
352   lateral longitudinal muscles centered around the 4th abdominal segment (A4) of the larval body
353   wall (Extended Data Fig. 1a). Each hemisegment was used as an internal control. A minimum
354   of 30 animals were scored per condition. Body wall muscle staining and quantification was
355   performed on animals from day 8 (CD), day 10 (early stage; HSD), day 14 (mid stage; HSD),
356   and day 16 (late stage; HSD) after egg laying.
357
358   **Microscopy and imaging.** Larval images were acquired with Leica M165 FC fluorescent
359   microscope equipped with Leica DFC 3000G digital camera. Confocal images were taken with
360   Leica SP5 II confocal microscope and Leica Application Suite Advanced Fluorescence software
361   (Leica Microsystems). Larval GFP/brightfield overlay images were compiled with Adobe
362   Photoshop software.
363
364   **Larval video tracking and analysis.** Larvae were maintained in normal culture conditions up
365   until the point of video recording. Individual larva were picked and placed onto the centre of
366   an agar plate at room temperature and recorded immediately. Video plate recordings were
367   carried out with use of a Teledyne DALSA Genie Nano Camera (G3-GM11-M2420) using
368   Gecko GigE Video Recorder software (v2.0.3.1; www.visionexperts.co.uk), at 25 frames per
369   second, ensuring a sharp contrast between the larva and background. 20 individual larvae
370   were recorded per condition up to a maximum of 5 minutes or until the larva was no longer
371   in the field of view (FOV). Individual videos–each corresponding to one larva–were segmented,
372   tracked and skeletonised using Tierpsy Tracker[12]. Data were discarded from subsequent analysis
373   if video tracking proved unsuccesssful, which occurred when the head was incorrectly identified
374   in 12 videos. When the head was correctly identified it was stable over the course of the video.
375   256 defined features, previously determined to be useful in classifying behaviour in *C.elegans*,

376 were extracted from the tracking data and compared between conditions[13]. Correction for
377 multiple testing was applied using the Benjamini–Hochberg procedure to control the false
378 discovery rate to 0.05[31].

380 **Quantitative RT-PCR.** Larvae were washed in PBS and dissected in RNALater solution. Total
381 RNA was extracted from pooled dissected tissue using the QIAGEN RNeasy Mini Kit. First-
382 strand DNA was synthesised with the iScript cDNA synthesis kit (Bio-Rad). PCR was performed
383 by mixing cDNA samples with iTaq Universal SYBR Green Supermix (Bio-Rad), ROX passive
384 reference dye (Bio-Rad) and the relevant primers in a 96-well plate. Analysis was carried out on
385 a 7900HT real-time PCR system (Applied Biosystems). At least 3 independent biological
386 replicates and 2 technical replicates were used. Expression values were normalised to *RpL32* or
387 *Act88F*. Primers used are listed in Extended Data Table 1.

389 **RNA-Sequencing.** RNA from pooled dissected tissue was extracted with the QIAGEN RNeasy
390 Mini Kit. A minimum of 3 samples were prepared for each genotype. RNA-seq libraries were
391 prepared from a minimum of 10ng of total RNA using the Illumina Truseq mRNA stranded
392 library prep kit (Illumina, San Diego, USA) according to the manufacturer's protocol. Library
393 quality was checked on a Bioanalyser HS DNA chip and concentrations were estimated by Qubit
394 measurement. Libraries were pooled in equimolar quantities and sequenced on a Hiseq2500
395 using paired end 100bp reads. At least 35 million reads passing filter were achieved per sample.
396 After demultiplexing, raw or trimmed RNA-Seq reads were aligned against Ensembl *Drosophila*
397 genome reference sequence assembly (dm3) and transcript annotations using TopHat2[32]. Trim
398 Galore, developed at The Babraham Institute by Felix Krueger
399 (http://www.bioinformatics.babraham.ac.uk/projects/trim_galore/), was applied for trimming
400 adapter and low quality reads. For differential gene expression analysis, gene-based read counts
401 were then obtained using the featureCounts function from Rsubread Bioconductor package[33].
402 Differential expression analysis was performed on the counts data using DESeq2 Bioconductor
403 package[34]. From tumour RNA-sequencing data, putative tumour-secreted factors were annotated
404 based on identification of genes labelled with the GO term 'extracellular' or presence of the
405 signal peptide sequence as identified by the signal peptide database
406 (http://www.signalpeptide.de).

408 **Gene Set Enrichment Analysis.** GSEA was carried out using a ranked gene list based on
409 Wald statistics from DESeq2 results[35]. MSigDB gene sets from 'H', 'C2' and 'C5' collections
410 were used and only considered where FDR q value <0.25. Normalised enrichment scores were
411 calculated for multiple terms within functional categories. Results were displayed as
412 cumulative normalised enrichment score, as previously published[36].

414 **Hemolymph sample preparation for metabolomic analyses.** Pooled hemolymph was
415 collected from multiple animals on ice to a combined minimum sample volume of 25 μl. Each
416 sample was mixed with 225 μL of methanol containing internal standards (50 μM). Then,
417 chloroform (250 μL) and Milli-Q water (100 μL) were added, mixed and centrifuged. The water
418 layer was filtrated through a 5-kDa cut-off filter to remove macromolecules. Filtrate was
419 centrifugally concentrated and resuspended in 25 μL of ultrapure water prior to measurement.
420 n=4 per condition.

422 **Metabolomic analyses.** Targeted metabolomic analyses were performed by the Human
423 Metabolome Technologies Inc., Yamagata, Japan. Capillary electrophoresis mass spectrometry
424 (CE-MS) was performed using Agilent CE-TOFMS Machine (CE-TOFMS) and Agilent 6460
425 TripleQuad LC/MS Machine (CE-QqQMS)(Agilent Technologies). Compounds were measured

426 based on previously described methods[37-39]. Peaks detected in CE-TOFMS analysis were
427 extracted using automatic integration software (MasterHands ver.2.17.1.11 developed at Keio
428 University)[40] and those in CE-QqQMS analysis were extracted using automatic integration
429 software (MassHunter Quantitative Analysis B.06.00 Agilent Technologies, Santa Clara, CA,
430 USA) in order to obtain peak information including m/z, migration time (MT), and peak area.
431 Putative metabolites were assigned from peak alignments based on the HMT metabolite database
432 on the basis of m/z and MT. Relative peak values were calculated based on internal standards
433 and normalised to sample volumes. Absolute quantification was calculated by normalising the
434 peak area of each metabolite with respect to the area of the internal standard and by using
435 standard curves, which were obtained by three-point calibrations. For hemolymph samples, 214
436 metabolites (135 metabolites in cation mode and 79 metabolites in anion mode respectively)
437 were annotated based on the HMT metabolite database, including 3-methylhistidine and proline.
438

439 **Human cancer database analyses.** TCGA IlluminaHiSeq_RNASeqV2 datasets for Colon
440 Adenocarcinoma (COAD), Stomach Adenocarcinoma (STAD), Pancreatic Adenocarcinoma
441 (PAAD), Rectum Adenocarcinoma (READ), Liver Hepatocellular Carcinoma (LIHC), Kidney
442 Renal Clear Cell Carcinoma (KIRC), Kidney Chromophobe (KICH) and Kidney Renal Papillary
443 Cell Carcinoma (KIRP) were obtained via the GDC Legacy Archive. Corresponding patient
444 clinical data, including overall survival status was obtained from cBioPortal for Cancer
445 Genomics (http://www.cbioportal.org.)[41,42]. When combining overlapping data from both
446 datasets the following number of patients remained and were analysed with respect to each
447 cancer type: (COAD – 177; STAD - 261; PAAD – 179; READ – 66; LIHC – 373; KIRC – 534;
448 KICH – 66 and KIRP - 291). The three kidney cancer tumour types (KIRC, KICH and KIRP)
449 were combined into a pooled kidney cancer group with a total of 891 patients.

450 Gene expression values were taken from the RSEM RNA-Sequencing data. The R/Bioconductor
451 package edgeR (3.22.3) was applied for trimmed mean of M-values (TMM) normalisation with
452 the calcNormFactors function. The function voom from R/Bioconductor package limma (3.36.3)
453 was used for converting raw counts to a log2 scale (counts per million). Individual patients were
454 assigned a Cachexia Score based on median expression levels of the following cachectic factors:
455 IL-1A, IL-1B, IL-6, IL-8 and TNF-α. Pearson correlation coefficients were calculated for six
456 cancer types between the Cachexia Score and expression of either SLC36A1 or SLC36A4. The
457 SLC36A2 and SLC36A3 isoforms of the SLC36A gene were excluded from analysis due to their
458 low expression levels across the tumour types examined. The Benjamini & Hochberg adjusted
459 p-value was calculated to measure the statistical significance of observed correlations as denoted
460 by the False Discovery Rate (FDR)[31].

461 For cancer types where statistically significant positive correlation was observed (FDR<0.05),
462 we defined two patient groups—(i) with high Cachexia Score and high SLC36 transporter
463 expression (High; red) and (ii) with low Cachexia Score and low SLC36 transporter expression
464 (Low; blue). Each group represents the upper (High) and lower (Low) quartile of patients in each
465 cancer type, as calculated from linear regression analysis using SLC36 expression level as the
466 explanatory variable. Kaplan-Meier survival curves were used to compare survival outcomes
467 between the High and Low patient groups within each cancer type[43]. The Log Rank test was used
468 to assess the statistical significance of survival curves and calculated p-values are displayed.
469

470 **Statistical methods.** Unless otherwise stated, all statistical analyses were carried out with an
471 unpaired, two-tailed students t-test in GraphPad Prism software (v.7.0d) where $p<0.005 = ***$;
472 $0.005<p<0.025 = **$; $0.025<p<0.05 = *$.
473

REFERENCES

1   Hosios, A. M. *et al.* Amino Acids Rather than Glucose Account for the Majority of Cell Mass in Proliferating Mammalian Cells. *Dev Cell* **36**, 540-549, doi:10.1016/j.devcel.2016.02.012 (2016).

2   Jain, M. *et al.* Metabolite profiling identifies a key role for glycine in rapid cancer cell proliferation. *Science* **336**, 1040-1044, doi:10.1126/science.1218595 (2012).

3   Sahu, N. *et al.* Proline Starvation Induces Unresolved ER Stress and Hinders mTORC1-Dependent Tumorigenesis. *Cell Metab* **24**, 753-761, doi:10.1016/j.cmet.2016.08.008 (2016).

4   Olivares, O. *et al.* Collagen-derived proline promotes pancreatic ductal adenocarcinoma cell survival under nutrient limited conditions. *Nat Commun* **8**, 16031, doi:10.1038/ncomms16031 (2017).

5   Commisso, C. *et al.* Macropinocytosis of protein is an amino acid supply route in Ras-transformed cells. *Nature* **497**, 633-637, doi:10.1038/nature12138 (2013).

6   Fearon, K. C., Glass, D. J. & Guttridge, D. C. Cancer cachexia: mediators, signaling, and metabolic pathways. *Cell Metab* **16**, 153-166, doi:10.1016/j.cmet.2012.06.011 (2012).

7   Petruzzelli, M. & Wagner, E. F. Mechanisms of metabolic dysfunction in cancer-associated cachexia. *Genes Dev* **30**, 489-501, doi:10.1101/gad.276733.115 (2016).

8   Schmidt, S. F., Rohm, M., Herzig, S. & Diaz, M. B. Cancer Cachexia: More Than Skeletal Muscle Wasting. *Trends Cancer* **4**, 849-860, doi:10.1016/j.trecan.2018.10.001 (2018).

9   Hirabayashi, S., Baranski, T. J. & Cagan, R. L. Transformed Drosophila cells evade diet-mediated insulin resistance through wingless signaling. *Cell* **154**, 664-675, doi:10.1016/j.cell.2013.06.030 (2013).

10   Hirabayashi, S. & Cagan, R. L. Salt-inducible kinases mediate nutrient-sensing to link dietary sugar and tumorigenesis in Drosophila. *Elife* **4**, e08501, doi:10.7554/eLife.08501 (2015).

11   Musselman, L. P. *et al.* A high-sugar diet produces obesity and insulin resistance in wild-type Drosophila. *Dis Model Mech* **4**, 842-849, doi:10.1242/dmm.007948 (2011).

12   Javer, A. *et al.* An open-source platform for analyzing and sharing worm-behavior data. *Nat Methods* **15**, 645-646, doi:10.1038/s41592-018-0112-1 (2018).

13   Javer, A., Ripoll-Sanchez, L. & Brown, A. E. X. Powerful and interpretable behavioural features for quantitative phenotyping of Caenorhabditis elegans. *Philos Trans R Soc Lond B Biol Sci* **373**, doi:10.1098/rstb.2017.0375 (2018).

14   Haas, K. F., Woodruff, E., 3rd & Broadie, K. Proteasome function is required to maintain muscle cellular architecture. *Biol Cell* **99**, 615-626, doi:10.1042/BC20070019 (2007).

15   Vattemi, G., Engel, W. K., McFerrin, J. & Askanas, V. Endoplasmic reticulum stress and unfolded protein response in inclusion body myositis muscle. *Am J Pathol* **164**, 1-7, doi:10.1016/S0002-9440(10)63089-1 (2004).

16   Tipton, K. D., Hamilton, D. L. & Gallagher, I. J. Assessing the Role of Muscle Protein Breakdown in Response to Nutrition and Exercise in Humans. *Sports Med* **48**, 53-64, doi:10.1007/s40279-017-0845-5 (2018).

17   Nowak, K., Seisenbacher, G., Hafen, E. & Stocker, H. Nutrient restriction enhances the proliferative potential of cells lacking the tumor suppressor PTEN in mitotic tissues. *Elife* **2**, e00380, doi:10.7554/eLife.00380 (2013).

18   Katheder, N. S. *et al.* Microenvironmental autophagy promotes tumour growth. *Nature* **541**, 417-420, doi:10.1038/nature20815 (2017).

11

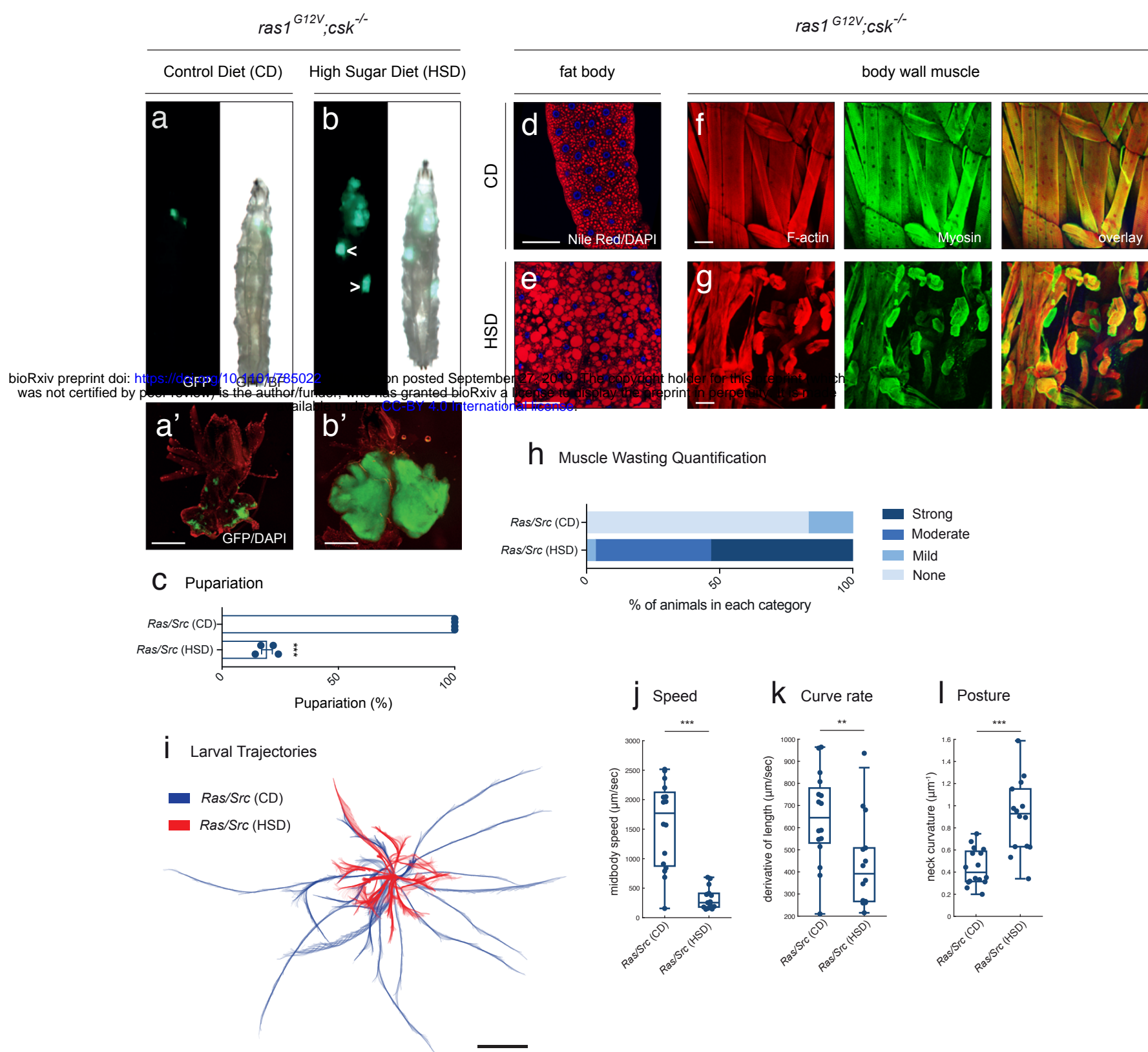| 524 | 19 | Lin, W. Y. *et al.* The SLC36 transporter Pathetic is required for extreme dendrite growth in Drosophila sensory neurons. *Genes Dev* **29**, 1120-1135, doi:10.1101/gad.259119.115 (2015). |
527	20	Ikmi, A. *et al.* Molecular evolution of the Yap/Yorkie proto-oncogene and elucidation of its core transcriptional program. *Mol Biol Evol* **31**, 1375-1390, doi:10.1093/molbev/msu071 (2014).
530	21	Thwaites, D. T. & Anderson, C. M. The SLC36 family of proton-coupled amino acid transporters and their potential role in drug transport. *Br J Pharmacol* **164**, 1802-1816, doi:10.1111/j.1476-5381.2011.01438.x (2011).
533	22	Figueroa-Clarevega, A. & Bilder, D. Malignant Drosophila tumors interrupt insulin signaling to induce cachexia-like wasting. *Dev Cell* **33**, 47-55, doi:10.1016/j.devcel.2015.03.001 (2015).
536	23	Kwon, Y. *et al.* Systemic organ wasting induced by localized expression of the secreted insulin/IGF antagonist ImpL2. *Dev Cell* **33**, 36-46, doi:10.1016/j.devcel.2015.02.012 (2015).
539	24	Song, W. *et al.* Tumor-Derived Ligands Trigger Tumor Growth and Host Wasting via Differential MEK Activation. *Dev Cell*, doi:10.1016/j.devcel.2018.12.003 (2019).
541	25	Grifoni, D., Sollazzo, M., Fontana, E., Froldi, F. & Pession, A. Multiple strategies of oxygen supply in Drosophila malignancies identify tracheogenesis as a novel cancer hallmark. *Sci Rep* **5**, 9061, doi:10.1038/srep09061 (2015).
544	26	Cancer Genome Atlas, N. Comprehensive molecular characterization of human colon and rectal cancer. *Nature* **487**, 330-337, doi:10.1038/nature11252 (2012).
546	27	Johnston, A. J. *et al.* Targeting of Fn14 Prevents Cancer-Induced Cachexia and Prolongs Survival. *Cell* **162**, 1365-1378, doi:10.1016/j.cell.2015.08.031 (2015).
548	28	Metzner, L., Neubert, K. & Brandsch, M. Substrate specificity of the amino acid transporter PAT1. *Amino Acids* **31**, 111-117, doi:10.1007/s00726-005-0314-6 (2006).
550	29	Toyoshima, K. *et al.* Increased plasma proline concentrations are associated with sarcopenia in the elderly. *PLoS One* **12**, e0185206, doi:10.1371/journal.pone.0185206 (2017).
553	30	Loayza-Puch, F. *et al.* Tumour-specific proline vulnerability uncovered by differential ribosome codon reading. *Nature* **530**, 490-494, doi:10.1038/nature16982 (2016).
555	31	Benjamini, Y. & Hochberg, Y. Controlling the False Discovery Rate - a Practical and Powerful Approach to Multiple Testing. *J R Stat Soc B* **57**, 289-300 (1995).
557	32	Kim, D. *et al.* TopHat2: accurate alignment of transcriptomes in the presence of insertions, deletions and gene fusions. *Genome Biol* **14**, R36, doi:10.1186/gb-2013-14-4-r36 (2013).
560	33	Liao, Y., Smyth, G. K. & Shi, W. featureCounts: an efficient general purpose program for assigning sequence reads to genomic features. *Bioinformatics* **30**, 923-930, doi:10.1093/bioinformatics/btt656 (2014).
563	34	Anders, S. & Huber, W. Differential expression analysis for sequence count data. *Genome Biol* **11**, R106, doi:10.1186/gb-2010-11-10-r106 (2010).
565	35	Subramanian, A. *et al.* Gene set enrichment analysis: a knowledge-based approach for interpreting genome-wide expression profiles. *Proc Natl Acad Sci U S A* **102**, 15545-15550, doi:10.1073/pnas.0506580102 (2005).
568	36	Cuartero, S. *et al.* Control of inducible gene expression links cohesin to hematopoietic progenitor self-renewal and differentiation. *Nat Immunol* **19**, 932-941, doi:10.1038/s41590-018-0184-1 (2018).
571	37	Soga, T. & Heiger, D. N. Amino acid analysis by capillary electrophoresis electrospray ionization mass spectrometry. *Anal Chem* **72**, 1236-1241 (2000).

38   Soga, T. *et al.* Simultaneous determination of anionic intermediates for Bacillus subtilis metabolic pathways by capillary electrophoresis electrospray ionization mass spectrometry. *Anal Chem* **74**, 2233-2239 (2002).

39   Soga, T. *et al.* Quantitative metabolome analysis using capillary electrophoresis mass spectrometry. *J Proteome Res* **2**, 488-494 (2003).

40   Sugimoto, M., Wong, D. T., Hirayama, A., Soga, T. & Tomita, M. Capillary electrophoresis mass spectrometry-based saliva metabolomics identified oral, breast and pancreatic cancer-specific profiles. *Metabolomics* **6**, 78-95, doi:10.1007/s11306-009-0178-y (2010).

41   Cerami, E. *et al.* The cBio cancer genomics portal: an open platform for exploring multidimensional cancer genomics data. *Cancer Discov* **2**, 401-404, doi:10.1158/2159-8290.CD-12-0095 (2012).

42   Gao, J. *et al.* Integrative analysis of complex cancer genomics and clinical profiles using the cBioPortal. *Sci Signal* **6**, pl1, doi:10.1126/scisignal.2004088 (2013).

43   Kaplan, E. L. Citation Classic - Nonparametric-Estimation from Incomplete Observations. *Cc/Life Sci*, 14-14 (1983).

ACKNOWLEDGEMENTS

AUTHOR CONTRIBUTIONS

H.N., L.C., A.E.X.B. and S.H. performed and analysed experiments. Y-F. W. carried out bioinformatics analysis. H.N. and S.H. conceived and designed the project and wrote the manuscript, with all authors providing feedback.

Figure 1. HSD-fed Ras/Src-animals exhibit cachexia-like muscle wasting and associated locomotion defects.

a, b, *ras1^G12V^;csk^-/-* third-instar larvae fed a CD (**a**) or HSD (**b**). Transformed tissue is labelled with GFP (green). Secondary tumours are observed in a subset of animals (arrowheads in **b**). **a', b',** Matching dissected eye epithelial tissue stained with DAPI (red). Scale bar, 250 μm. **c**, Pupariation percentage of *ras1^G12V^;csk^-/-* animals raised on CD or HSD. Results are shown as mean ± SEM of four independent experiments with n≥10 animals for each data point. Asterisks indicate statistically significant difference (***; p<0.005). **d, e,** Nile Red (red) and DAPI (blue) staining of dissected fat body tissue from *ras1^G12V^;csk^-/-* third-instar larvae fed a CD (**d**) or HSD (**e**). Scale bar, 100 μm. **f, g,** F-actin (red) and anti-myosin (green) staining of dissected larval body wall muscle tissue from *ras1^G12V^;csk^-/-* third-instar larvae fed a CD (**f**) or HSD (**g**). Scale bar, 100 μm. **h**, Matching body wall muscle wasting quantification. n≥30 per condition. **i**, Individual larval trajectories from video tracking analysis of *ras1^G12V^;csk^-/-* third-instar larvae fed a CD, or HSD. Scale bar, 1 cm. **j-l,** Average midbody speed (**j**), body curvature (**k**), and body posture (**l**) of *ras1^G12V^;csk^-/-* third-instar larvae fed a CD, or HSD with results shown as mean ± SEM with each data point representing one individual animal. Asterisks indicate statistically significant difference (***; p<0.005, **; 0.005<p<0.025).

Figure 2. *Drosophila* **SLC36-family amino acid transporters Path and CG1139 are required for obesity-enhanced Ras/Src tumour growth.**

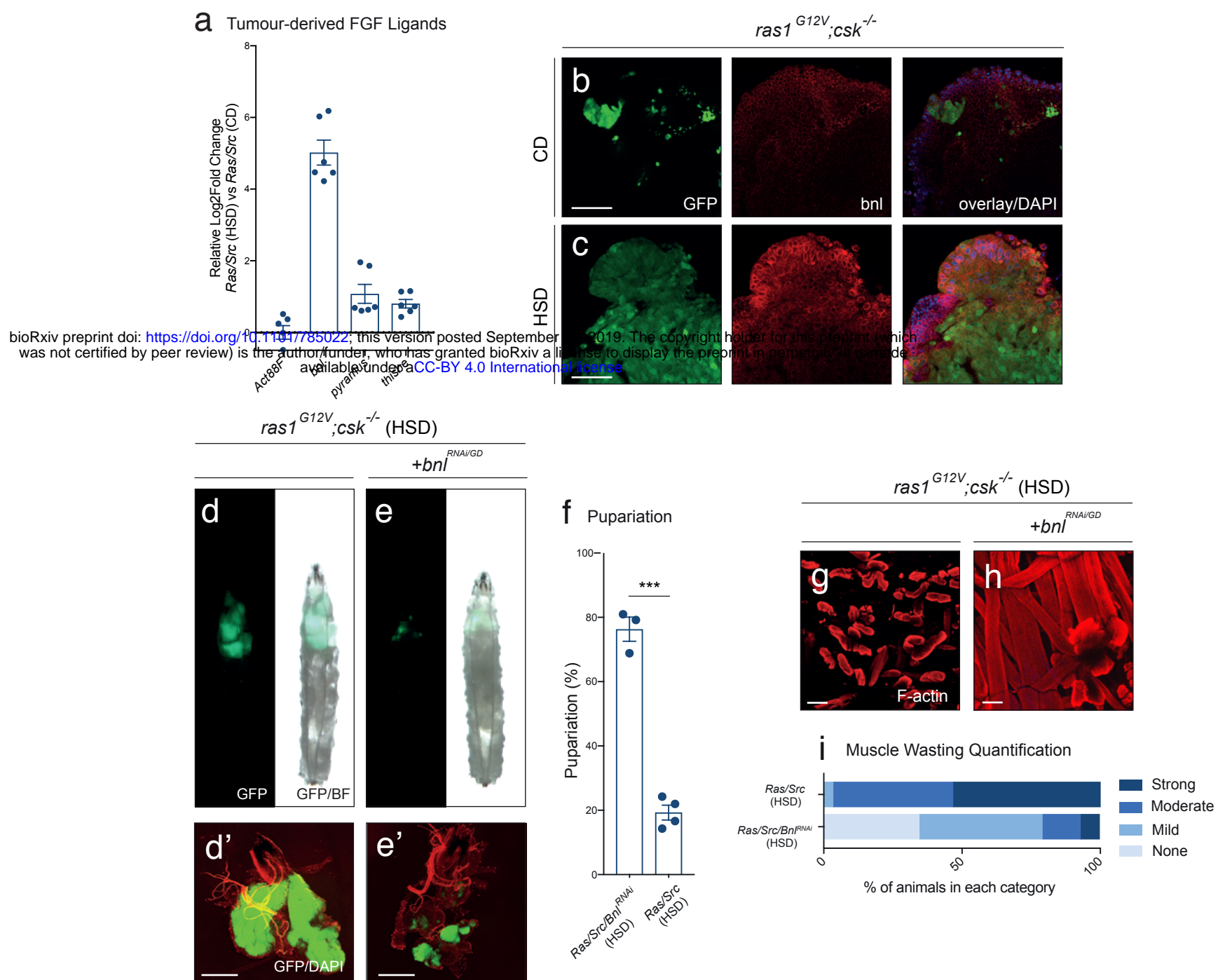**a**, Circulating hemolymph levels of upregulated amino acids in $ras1^{G12V};csk^{-/-}$ animals raised on HSD compared to $ras1^{G12V};csk^{-/-}$ animals raised on CD. Results are shown as mean relative fold change from $ras1^{G12V};csk^{-/-}$ animals raised on HSD vs. CD. **b**, Relative log2fold change of SLC7 and SLC36 family amino acid transporters in dissected tumour tissue from $ras1^{G12V};csk^{-/-}$ animals raised on HSD compared to $ras1^{G12V};csk^{-/-}$ animals raised on CD, as determined by qPCR. Samples are normalised to *Act88F*. Results are shown as mean ± SEM. **c-j**, Dissected eye epithelial tissue stained with DAPI (red) from $ras1^{G12V};csk^{-/-}$ animals raised on HSD (**c**), with *mnd^RNAi^* (**d**), *Jhl-21^RNAi^* (**e**), *CG5535^RNAi^* (**f**), *slif^RNAi^* (**g**), *CG8785^RNAi^* (**h**), *path^RNAi^* (**i**), and *CG1139^RNAi^* (**j**). Scale bar, 250 μm. **k-m**, Dissected eye epithelial tissue stained with DAPI (red) from $ras1^{G12V};csk^{-/-}$ animals raised on CD (**k**), with *path^RNAi^* (**l**), and *CG1139^RNAi^* (**m**). Scale bar, 250 μm. **n-p**, Anti-Path staining (red) of dissected tumour tissue from $ras1^{G12V};csk^{-/-}$ animals raised on CD (**n**), $ras1^{G12V};csk^{-/-}$ animals raised on HSD (**o**), and $ras1^{G12V};csk^{-/-},wts$ animals raised on HSD (**p**) with DAPI (blue). Scale bar, 100 μm. **q-s**, Anti-CG1139 staining (red) of dissected tumour tissue from $ras1^{G12V};csk^{-/-}$ animals raised on CD (**q**), $ras1^{G12V};csk^{-/-}$ animals raised on HSD (**r**), and $ras1^{G12V};csk^{-/-},wts$ animals raised on HSD (**s**) with DAPI (blue). Scale bar, 100 μm.
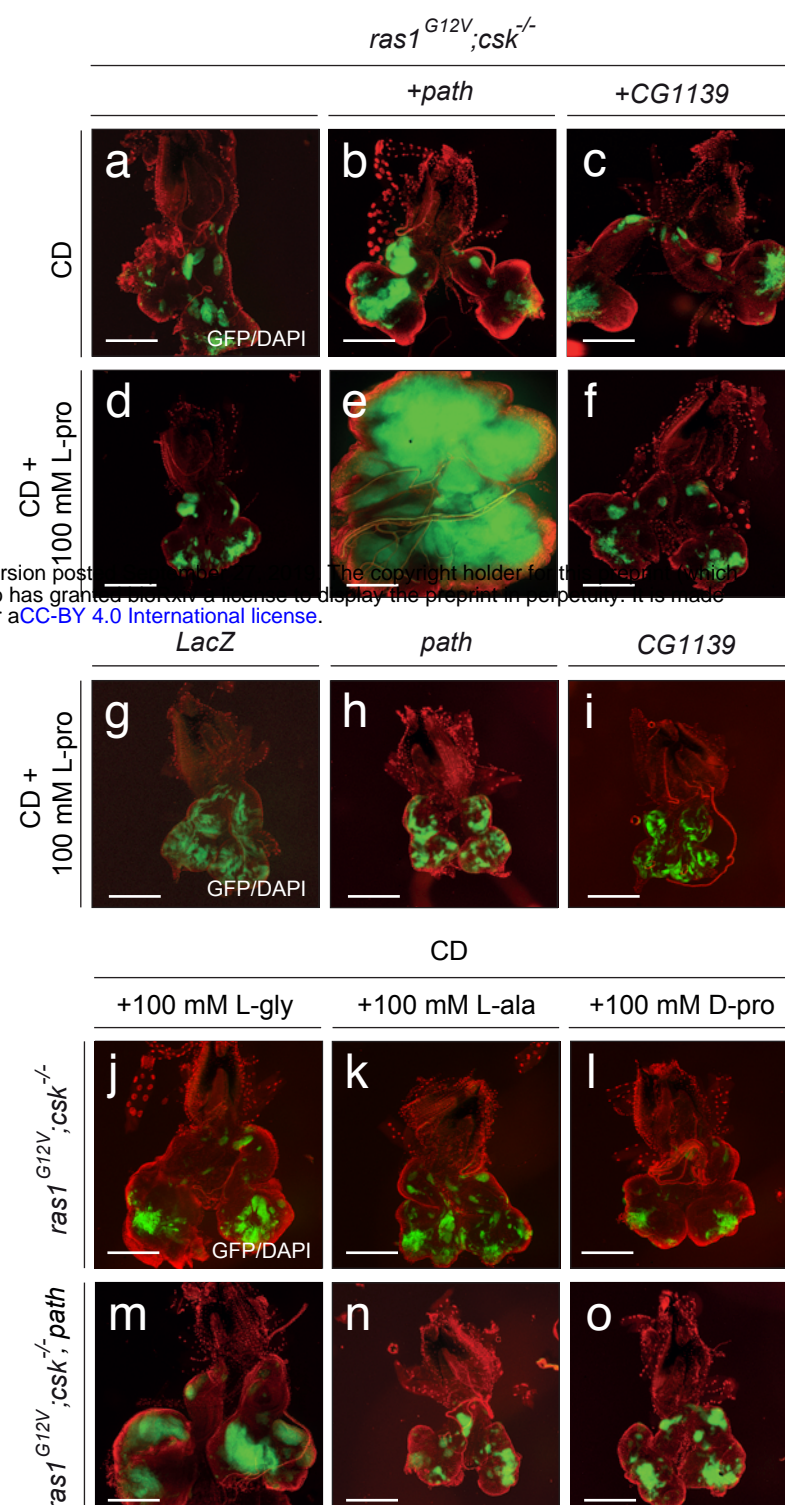
Figure 3. Proline promotes Ras/Src-tumour growth through amino acid transporter Path.

a-c, Dissected eye epithelial tissue stained with DAPI (red) from $ras1^{G12V};csk^{-/-}$ animals (**a**), $ras1^{G12V};csk^{-/-},PathA$ animals (**b**), and $ras1^{G12V},CG1139;csk^{-/-}$ animals (**c**) raised on CD. Scale bar, 250 μm. **d-f,** Dissected eye epithelial tissue stained with DAPI (red) from $ras1^{G12V};csk^{-/-}$animals (**d**), $ras1^{G12V};csk^{-/-},PathA$ animals (day 10 AEL) (**e**), and $ras1^{G12V},CG1139;csk^{-/-}$ animals (**f**) raised on CD supplemented with 100 mM L-proline. Scale bar, 250 μm. **g-i,** Dissected eye epithelial tissue stained with DAPI (red) from $LacZ$ animals (**g**), $PathA$ animals (**h**), and $CG1139$ animals (**i**) raised on CD supplemented with 100 mM L-proline. Scale bar, 250 μm. **j-l,** Dissected eye epithelial tissue stained with DAPI (red) from $ras1^{G12V};csk^{-/-}$ animals raised on CD supplemented with 100 mM L-glycine (**j**), 100 mM L-alanine (**k**), and 100 mM D-proline (**l**). Scale bar, 250 μm. **m-o,** Dissected eye epithelial tissue stained with DAPI (red) from $ras1^{G12V};csk^{-/-},PathA$ animals raised on CD supplemented with 100 mM L-glycine (**m**), 100 mM L-alanine (**n**), and 100 mM D-proline (**o**). Scale bar, 250 μm.

Figure 4. Tumour-derived branchless mediates muscle wasting and subsequent tumour growth.

a, Relative log2fold change of *Drosophila* fibroblast growth factors, *branchless* (*bnl*), *pyramus* and *thisbe* in dissected tumour tissue from *ras1^{G12V};csk^{-/-}* animals raised on HSD compared to *ras1^{G12V};csk^{-/-}* animals raised on CD, as determined by qPCR. Samples are normalised to *Act88F*. Results are shown as mean ± SEM. **b, c,** Anti-Bnl staining (red) of dissected tumour tissue from *ras1^{G12V};csk^{-/-}* animals raised on CD (**b**) or HSD (**c**) with DAPI (blue). Scale bar, 40 μm. **d, e,** Third-instar larvae from *ras1^{G12V};csk^{-/-}* (**d**), and *ras1^{G12V};csk^{-/-},bnl^{RNAi}* (**e**). **d', e',** Matching dissected eye epithelial tissue stained with DAPI (red). Scale bar, 250 μm. **f,** Pupariation percentage of animals raised on HSD. Results are shown as mean ± SEM of independent experiments with n≥10 animals for each data point. Asterisks indicate statistically significant difference (***; p<0.005). **g, h,** Matching dissected larval body wall muscle. Scale bar, 100 μm. **i,** Matching body wall muscle wasting quantification. n≥30 per condition.

**a** Pearson coefficients for Cachexia Score correlations

	Kidney n=891		Pancreatic n=179		Liver n=373		Colon n=177		Rectal n=66		Stomach n=261	
	Correlation	FDR	Correlation	FDR	Correlation	FDR	Correlation	FDR	Correlation	FDR	Correlation	FDR
SLC36A1	0.2576	6.76E-14	0.2358	0.0044	0.0683	0.2404	-0.0616	0.4270	-0.2120	0.1499	0.1148	0.1499
SLC36A4	0.1856	2.37E-08	-0.0509	0.4985	0.1675	0.0021	0.1262	0.1499	0.1412	0.3443	0.0597	0.4042
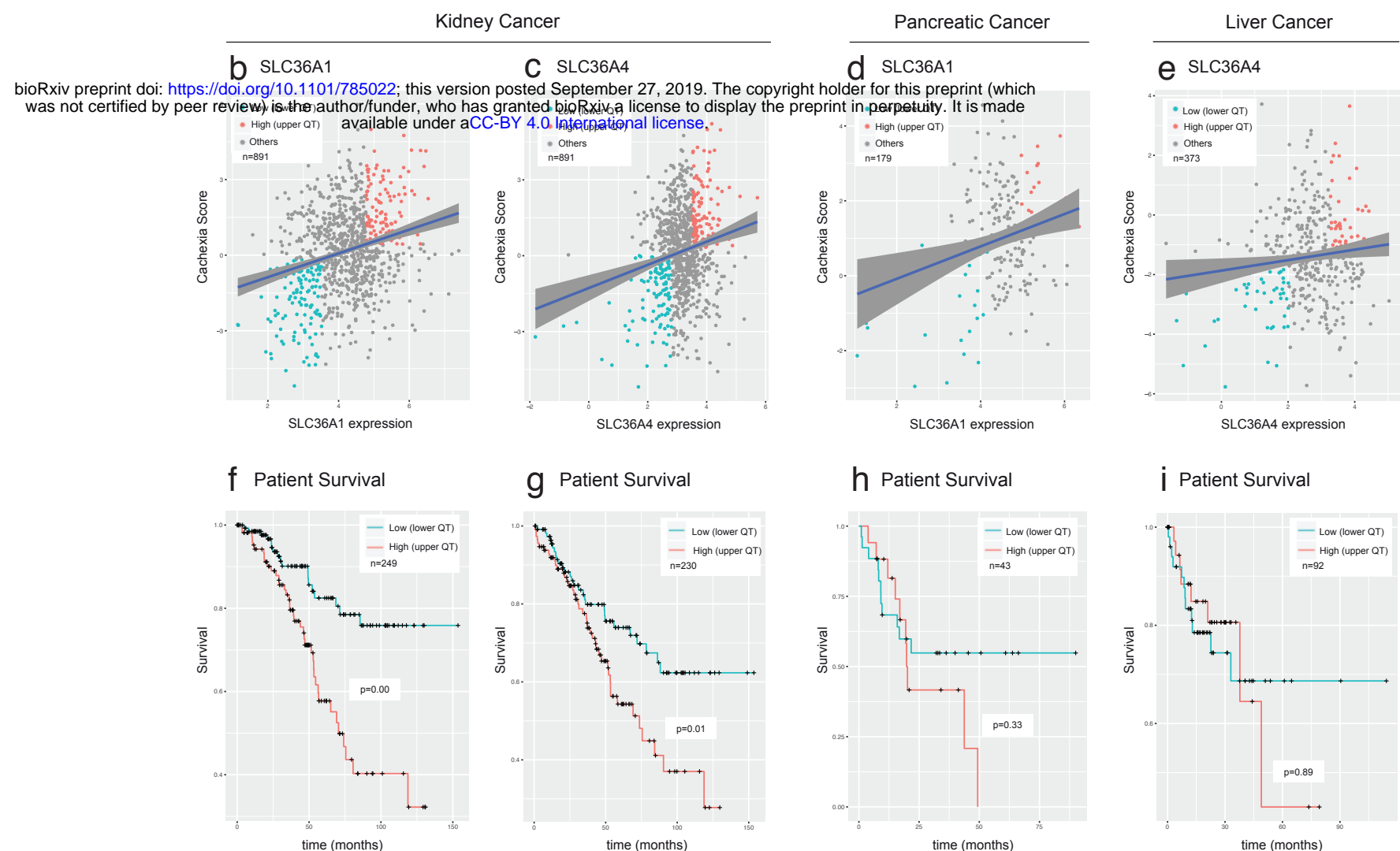
Figure 5. Coordinated induction of cachectic factors and SLC36-transporter expression decreases survival in kidney cancer patients.

a, Pearson correlation coefficients and associated false discovery rates (FDR) for observed correlation between Cachexia Score and SLC36A1 or SLC36A4 expression levels across kidney, pancreatic, liver, colon, rectal, and stomach cancer patient groups. Red denotes conditions with statistically significant positive correlation (FDR<0.05). **b-e,** Scatter plot and overlaid linear regression curve for Cachexia Score and SLC36A1 (**b**) or SLC36A4 (**c**) expression levels in kidney cancer (n=891), Cachexia Score and SLC36A1 expression in pancreatic cancer (n=179) (**d**), and Cachexia Score and SLC36A4 expression in liver cancer (n=373) (**e**). Blue data points denote the lower quartile of patients with low Cachexia Score and low SLC36; red data points denote the upper quartile of patients with high Cachexia Score and high SLC36 transporter expression; grey data points denote the 2nd and 3rd quartile of patients classified as 'Others'. **f-i**, Kaplan-Meier survival curve for the upper quartile of patients with high Cachexia Score and high transporter expression (High) and lower quartile of patients with low Cachexia Score and low transporter expression (Low). SLC36A1 patient groups in kidney cancer as defined in **b** (n=249) (**f**), SLC36A4 patient groups in kidney cancer as defined in **c** (n=230) (**g**), SLC36A1 patient groups in pancreatic cancer as defined in **d** (n=43) (**h**), and SLC36A4 patient groups in liver cancer as defined in **e** (n=92) (**i**).
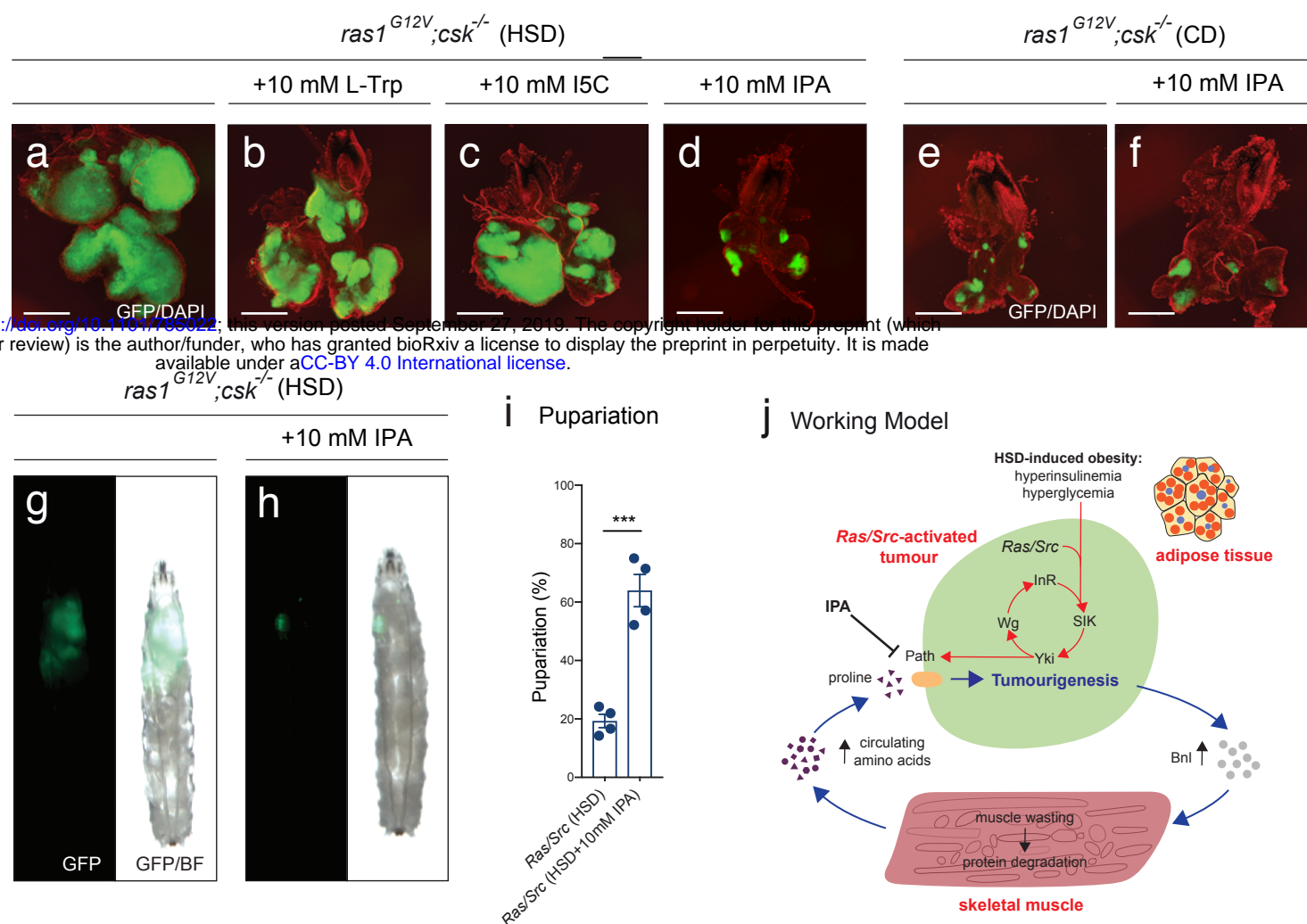
**Figure 6. Targeting proline vulnerability with amino acid derivatives suppresses tumour growth.**

a-d, Dissected eye epithelial tissue stained with DAPI (red) from $ras1^{G12V};csk^{-/-}$ animals raised on HSD (**a**), HSD supplemented with 10 mM L-tryptophan (**b**), HSD supplemented with 10 mM Indole-5-carboxylic acid (**c**), HSD supplemented with 10 mM Indole-3-propionic acid (IPA) (**d**). Scale bar, 250 μm. **e, f**, Dissected eye epithelial tissue stained with DAPI (red) from $ras1^{G12V};csk^{-/-}$ animals raised on CD (**e**), and CD supplemented with 10 mM IPA (**f**). Scale bar, 250 μm. **g, h**, Third-instar larvae from $ras1^{G12V};csk^{-/-}$ animals raised on HSD (**g**) and HSD supplemented with 10 mM Indole-3-propionic acid (IPA) (**h**). **i,** Pupariation percentage of $ras1^{G12V};csk^{-/-}$ animals raised on HSD and HSD supplemented with 10 mM IPA. Results are shown as mean ± SEM of four independent experiments with n≥10 animals for each data point. Asterisks indicate statistically significant difference (***; p<0.005). **j,** Working model illustrating dual-layered-coordination of tumour metabolic response: (i) at the whole organism level—Branchless (Bnl)-dependent induction of cachexia-like muscle wasting and systemic amino acid release (blue arrows)—and (ii) at the tumour-autonomous level—Yorkie-dependent induction of amino acid transporter expression (red arrows). The tumour-autonomous SIK-Yki-Wg-InR circuit was identified previously[10]. IPA represents a therapeutic strategy to break the nutritional circuit between muscle wasting and tumour growth by targeting the SLC36 family transporter Path. SIK; Salt-inducible kinase, Yki; Yorkie, Wg; Wingless, InR; Insulin Receptor, IPA; indole-3-propionic acid.
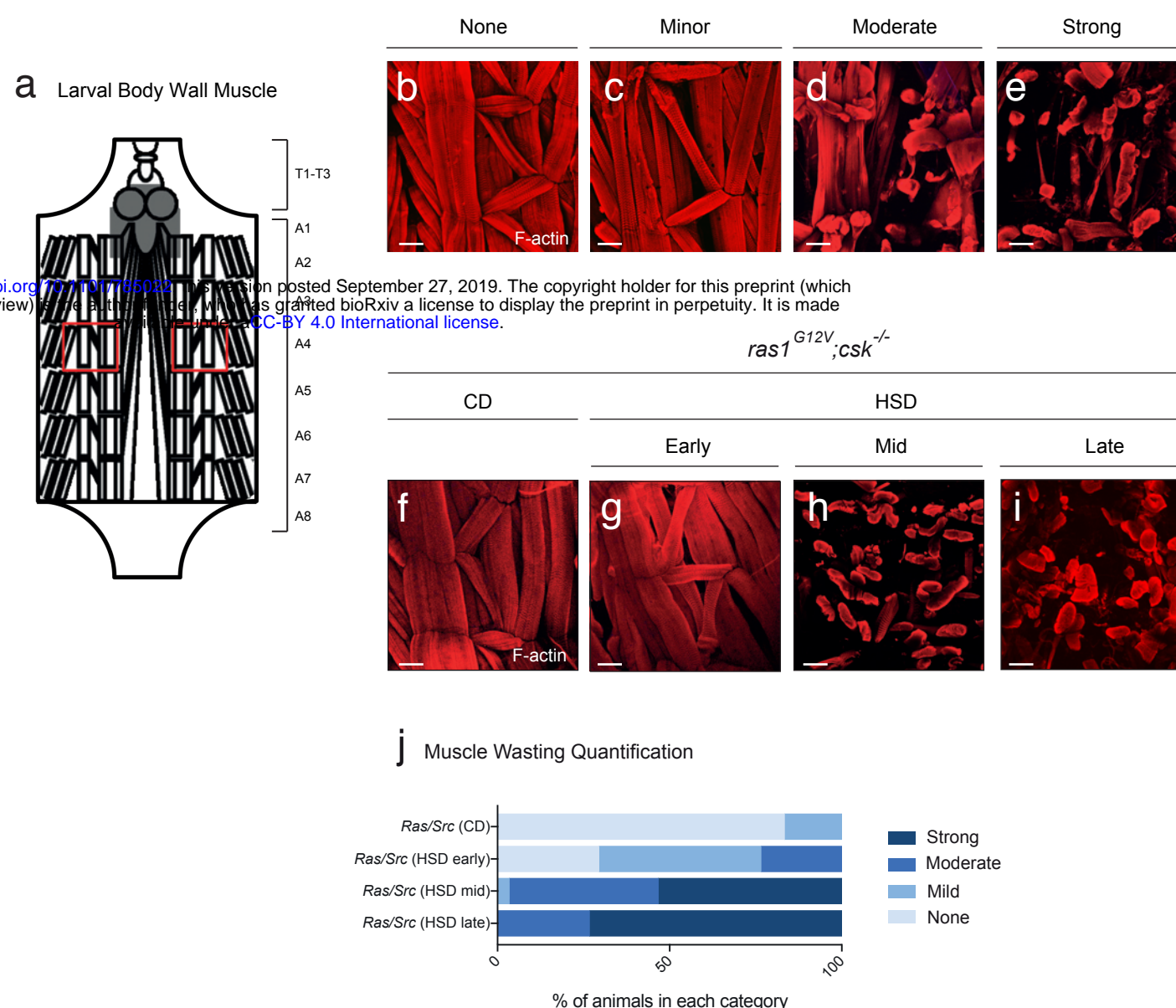
Extended Data Figure 1. HSD-fed Ras/Src-animals exhibit progressive cachexia-like muscle wasting.

a, Schematic of larval body wall muscle upon dissection from anterior (top) to posterior (bottom). The larval body wall contains 3 thoracic segments (T1-T3) and 9 abdominal segments (A1-A9). Abdominal muscles from segments A1-A8 are labelled. Red boxes outline regions of the body wall muscle which are imaged, containing the ventral longitudinal, lateral oblique and lateral longitudinal muscles centred around the fourth abdominal segment. **b-e**, Representative images of dissected larval body wall muscle stained with phalloidin to visualise F-actin. Muscle wasting scores increase in strength from left to right: "no wasting" (**b**), "minor" (**c**), "moderate" (**d**) and "strong" (**e**). Scale bar, 100 μm. **f-i**, Dissected larval body wall muscle of $ras1^{G12V};csk^{-/-}$ animals raised on CD (**f**) or on HSD at Early (**g**), Mid (**h**) and Late stage (**i**) Scale bar, 100 μm. **j**, Matching body wall muscle wasting quantification of $ras1^{G12V};csk^{-/-}$ animals raised on CD and HSD. X-axis represents the percentage of individual animals scoring in each category denoted "none", "mild", "moderate" or "strong". n≥30 per condition.
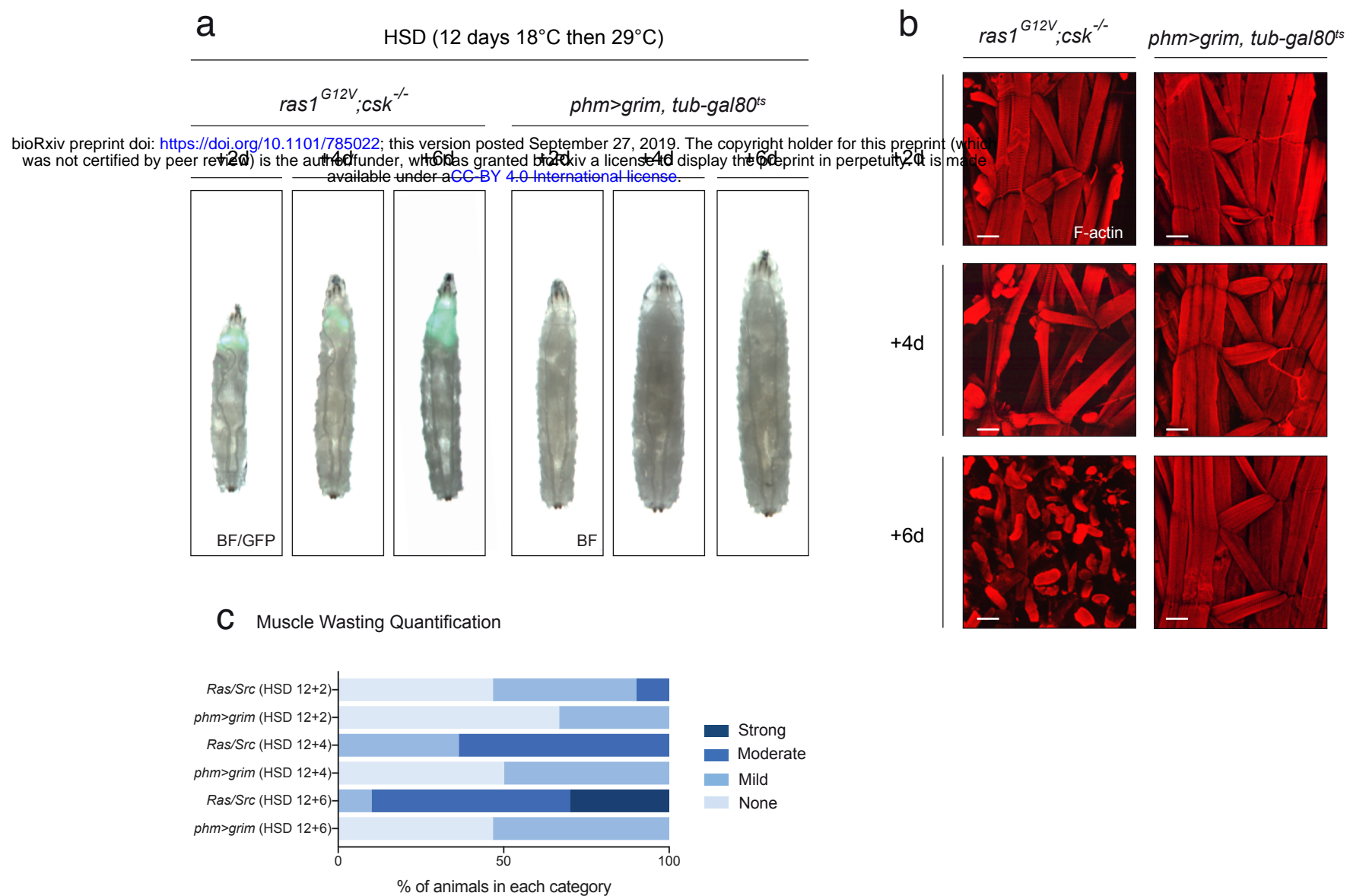
Extended Data Figure 2. Extended larval period is insufficient to account for systemic muscle wasting.

a, Third instar larvae of *ras1^G12V^;csk^-/-^* and *phm>grim, tub-gal80^ts^* animals raised on HSD for 12 days in 18°C plus 2, 4 and 6 days after temperature shift to 29°C (+2d, +4d and +6d respectively). *ras1^G12V^;csk^-/-^* animals are imaged under BF and GFP. *phm>grim* animals (tumour-free) are imaged under BF. **b**, Matching dissected larval body wall muscle. Scale bar, 100 μm. **c**, Matching body wall muscle wasting quantification. n≥30 per condition.
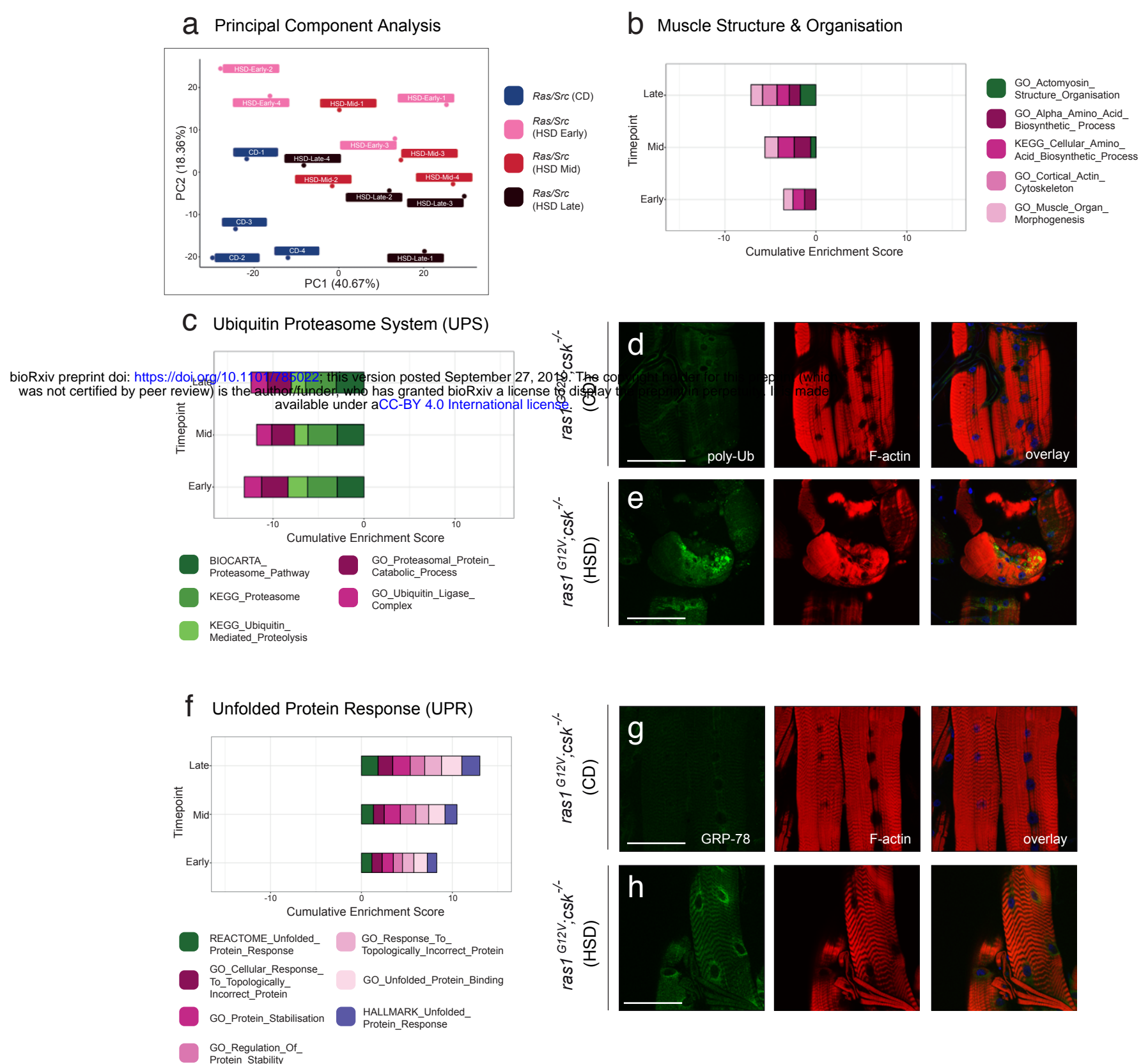
Extended Data Figure 3. HSD-fed Ras/Src-animals promote muscle wasting via proteasome dysfunction and unfolded protein response.

a, Principal Component Analysis of dissected muscle RNA-sequencing data from $ras1^{G12V};csk^{-/-}$ animals raised on CD (blue) and $ras1^{G12V};csk^{-/-}$ animals raised on HSD at Early (pink), Mid (red) and Late Stage (brown). n=4 per condition. **b**, Gene Set Enrichment Analysis (GSEA) for the functional category 'Muscle Structure & Organisation' from dissected muscle RNA-sequencing data from $ras1^{G12V};csk^{-/-}$ animals raised on HSD at Early Stage (Early), Mid Stage (Mid) and Late Stage (Late) compared to $ras1^{G12V};csk^{-/-}$ animals raised on CD. Data is displayed as cumulative enrichment score over the time course. Gene sets in purple are derived from Hallmark (H) datasets, gene sets in green are derived from Curated (C2) datasets and gene sets in pink are derived from Gene Ontology (C5) datasets. **c**, GSEA (as for **b**) for the functional category 'Ubiquitin Proteasome System'. **d, e**, Poly-Ubiquitin staining (green) of dissected body wall muscle from $ras1^{G12V};csk^{-/-}$ animals raised on CD (**d**) or HSD (**e**) and with DAPI (blue) and F-actin (red). Scale bar, 100 μm. **f**, GSEA (as for **b**) for the functional category 'Unfolded Protein Response'. **g, h**, GRP-78 staining (green) of dissected body wall muscle from $ras1^{G12V};csk^{-/-}$ animals raised on CD (**g**) or HSD (**h**) and with DAPI (blue) and F-actin (red). Scale bar, 100 μm.

a Principal Component Analysis
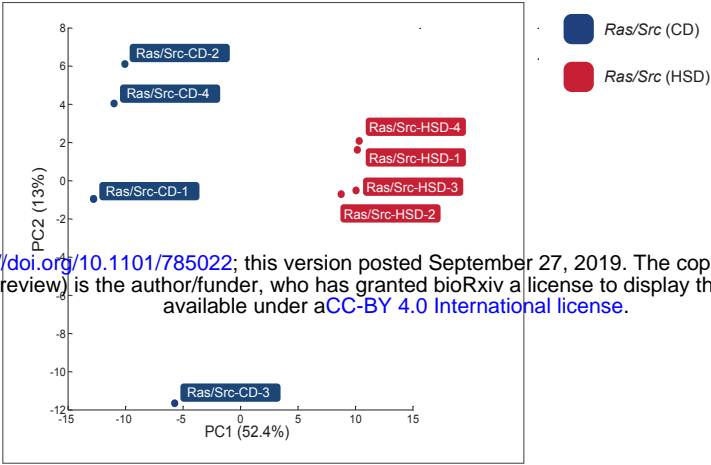
b Table of Amino Acids

| Compound	Absolute Concentration (µM)				HSD vs CD	
	CD		HSD			
	Mean	S.D	Mean	S.D	Ratio	p-value
Pro	8658	613	19584	1154	2.3	2.80E-05
Asp	112	29	221	94	2	0.099
His	4298	567	7902	736	1.8	3.30E-04
Ser	3831	567	6041	131	1.6	0.003
Ile	801	103	1083	127	1.4	1.50E-02
Leu	1250	158	1689	278	1.4	0.043
Ala	12?39	2339	14945	588	1.2	8.80E-02
Glu	5576	643	6806	919	1.2	0.076
Arg	2758	337	3339	342	1.2	5.20E-02
Val	2061	274	2453	255	1.2	0.083
Gln	25309	2317	28851	1207	1.1	4.70E-02
Lys	7198	1262	6836	337	0.9	0.614
Trp	470	57	427	36	0.9	2.53E-01
Asn	6771	620	5870	272	0.9	0.055
Phe	822	140	697	64	0.8	1.78E-01
Gly	7845	932	6528	199	0.8	0.063
Tyr	6183	1147	5041	843	0.8	1.64E-01
Thr	5666	1639	3834	267	0.7	0.11
Met	239	52	157	17	0.7	4.60E-02
Cys	7.4	5.9	N.A.	N.A.	<1	N.A.

c 3-methylhistidine
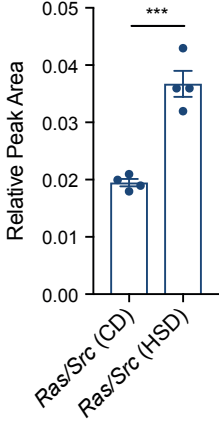
Extended Data Figure 4. Metabolomic analysis of hemolymph reveal an increase in circulating amino acids in HSD-fed Ras/Src-animals.

a, Principal Component Analysis of targeted metabolomic analysis from hemolymph in $ras1^{G12V};csk^{-/-}$ animals raised on CD (blue) or HSD (red). n=4 per condition. **b**, Amino acid concentrations from targeted metabolomic analysis of hemolymph in $ras1^{G12V};csk^{-/-}$ animals raised on CD (blue) or HSD (red). n=4 per condition. Amino acids are listed in order of highest fold-elevation in $ras1^{G12V};csk^{-/-}$ animals raised on HSD compared to CD. **c**, Circulating 3-methylhistidine levels depicted by relative peak area from hemolymph in $ras1^{G12V};csk^{-/-}$ animals raised on CD or HSD. Results are shown as mean ± SEM. Asterisks indicate statistically significant difference (***; p<0.005).

a Principal Component Analysis

b Amino Acid Transporters

$ras1^{G12V};csk^{-/-}$ (HSD)

$+path^{RNAi/TRiP}$ $+CG1139^{RNAi/KK}$

$ras1^{G12V}, path^{RNAi}; csk^{-/-}$ (HSD)

$ras1^{G12V}; csk^{-/-}, CG1139^{RNAi}$ (HSD)

Extended Data Figure 5. RNA-Seqencing identifies candidate amino acid transporters required for diet-enhanced tumour growth.
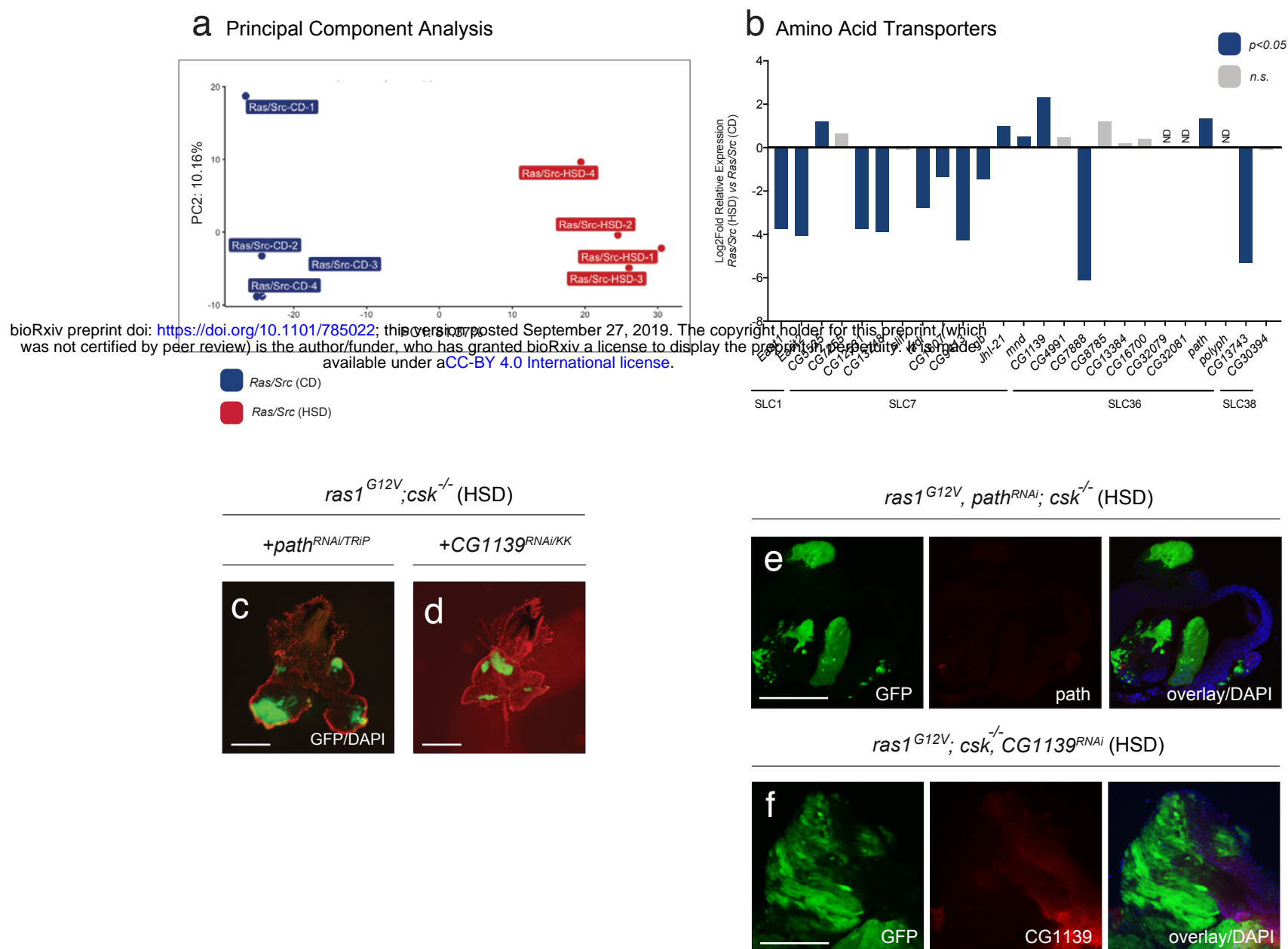
a, Principal Component Analysis of RNA-sequencing data from dissected tumour tissue in $ras1^{G12V};csk^{-/-}$ animals raised on CD (blue) or HSD (red). n=4 per condition. **b**, Expression levels of amino acid transporters of the SLC1, SLC7, SLC36, SLC38 families as measured by RNA-seq analysis. Gene expression levels are shown as the log2-relative fold change between $ras1^{G12V};csk^{-/-}$ animals raised on HSD compared to $ras1^{G12V};csk^{-/-}$ animals raised on CD. Blue bars indicate cases where p<0.05. Grey bars indicate cases where p>0.05. **c, d,** Dissected eye epithelial tissue stained with DAPI (red) from animals raised on HSD with independent RNAi lines, $ras1^{G12V},path^{RNAi/TRiP};csk^{-/-}$ (**c**) or $ras1^{G12V},CG1139^{RNAi/KK};csk^{-/-}$ (**d**). Scale bar, 250 μm. **e,** Anti-Path staining (red) of dissected tumour tissue from $ras1^{G12V}, path^{RNAi/KK};csk^{-/-}$ animals raised on HSD with DAPI (blue). Scale bar, 100 μm. **f**, Anti-CG1139 staining (red) of dissected tumour tissue from $ras1^{G12V};csk^{-/-},CG1139^{RNAi/GD}$ animals raised on HSD, with DAPI (blue). Scale bar, 100 μm.
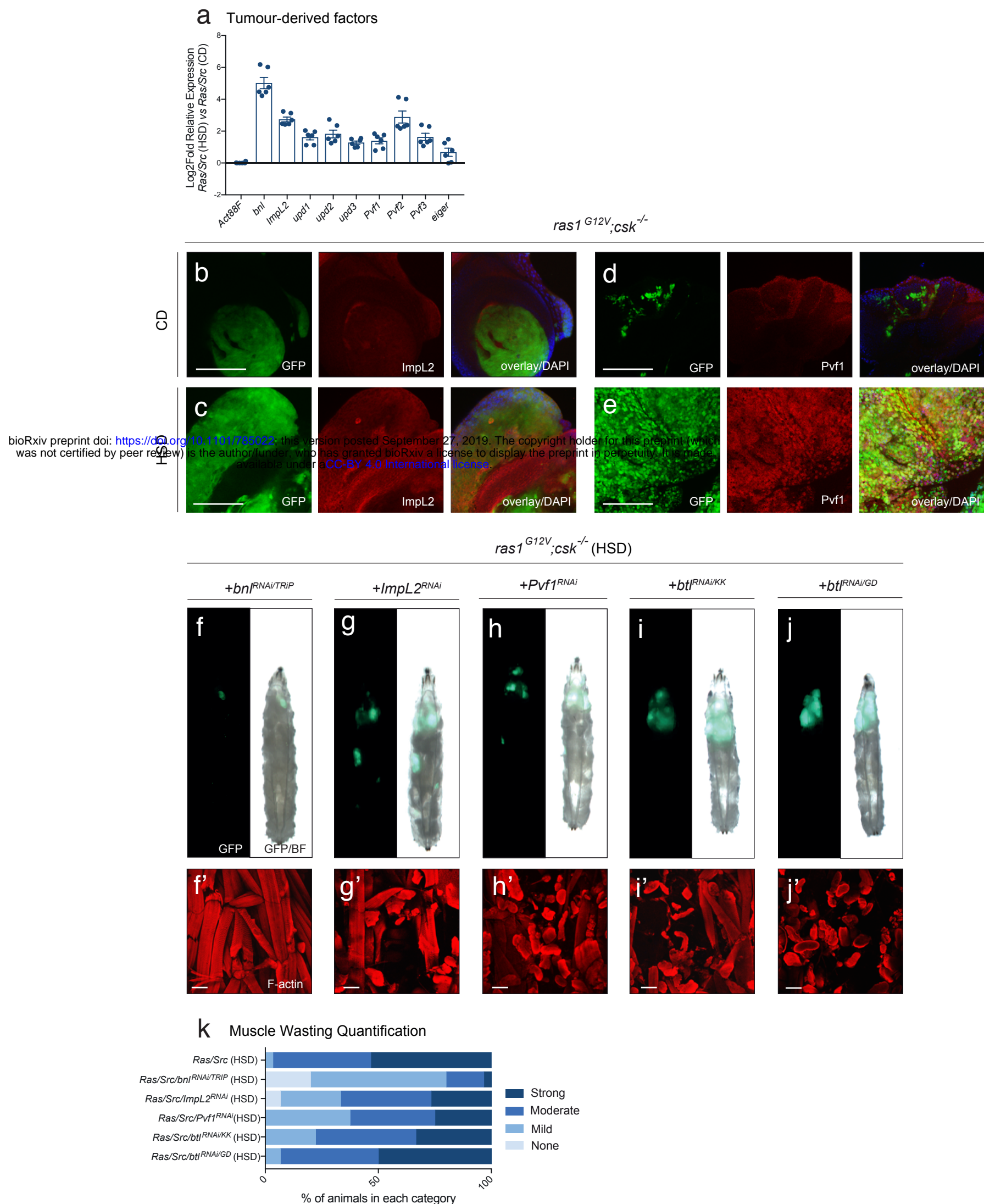
Extended Data Figure 6. RNA-Seqencing identifies branchless as a tumour-derived factor that contributes to muscle wasting and tumour growth.

a, qPCR validation of candidate tumour-derived factors—*bnl*, *ImpL2*, *upd1*, *upd2*, *upd3*, *Pvf1*, *Pvf2*, *Pvf3* and *eiger*—initially identified by RNA-sequencing. Gene expression levels are shown as log2-relative fold change between $ras1^{G12V};csk^{-/-}$ animals raised on HSD compared to $ras1^{G12V};csk^{-/-}$ animals raised on CD, as determined by qPCR. Samples are normalised to *Act88F*. Results are shown as mean ± SEM. **b, c,** ImpL2 staining (red) of dissected tumour tissue from $ras1^{G12V};csk^{-/-}$ animals raised on CD (**b**) or HSD (**c**) with DAPI (blue). Scale bar, 100 μm. **d, e,** Pvf1 staining (red) of dissected tumour tissue from $ras1^{G12V};csk^{-/-}$ animals raised on CD (**d**) or HSD (**e**) with DAPI (blue). Scale bar, 100 μm. **f-j,** $ras1^{G12V};csk^{-/-},bnl^{RNAi/TRIP}$ (**f**), $ras1^{G12V};csk^{-/-},ImpL2^{RNAi}$ (**g**), $ras1^{G12V};csk^{-/-},Pvf1^{RNAi}$ (**h**), $ras1^{G12V};csk^{-/-},btl^{RNAi/KK}$ (**i**), and $ras1^{G12V};csk^{-/-},btl^{RNAi/GD}$ (**j**) third-instar larvae raised on HSD. **f'-j',** Matching dissected larval body wall muscle. Scale bar, 100 μm. **k,** Matching body wall muscle wasting quantification. n≥30 per condition.
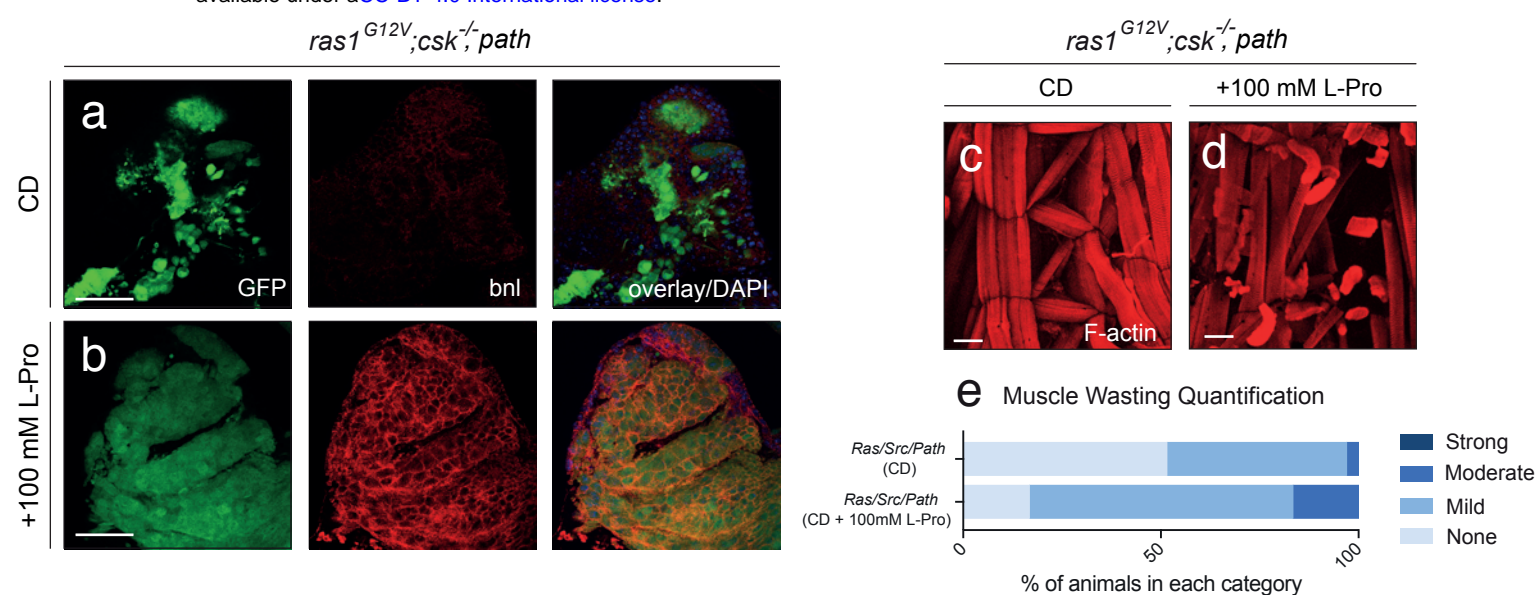
Extended Data Figure 7. Proline-mediated Ras/Src tumour growth promotes Bnl-expression and muscle wasting.
a, b, Anti-Bnl staining (red) of dissected tumour tissue from *ras1^{G12V};csk$^{-/-}$,PathA* animals raised on CD (**a**) or CD supplemented with 100mM proline (**b**) with DAPI (blue). Scale bar, 40 μm. **c, d,** Dissected larval body wall muscle from *ras1^{G12V};csk$^{-/-}$,PathA* animals raised on CD (**c**) or CD supplemented with 100mM proline (**d**). **e,** Matching body wall muscle wasting quantification. n≥30 per condition.

Gene	Forward (F) or Reverse (R)	Primers
RpL32	F	GCTAAGCTGTCGCACAAATG
	R	GTTCGATCCGTAACCGATGT
Act88F	F	TCGGCTCGGACAGTGATAGA
	R	AAGGATGAGCACCGACAACC
bnl	F	CTCAAGTTCCGAGGCCCAAG
	R	GGATGGCTCTTTTTCGGAGCA
pyramus	F	GGTTGGAAAGAGAAACGCCAC
	R	ACGCAGCACTGGATTGTAGG
thisbe	F	TTAGTTGGCATGAGGGAGCTG
	R	CAGATCGACAACGGAACGGA
ImpL2	F	AAGAGCCGTGGACCTGGTA
	R	TTGGTGAACTTGAGCCAGTCG
Pvf1	F	GCGCAGCATCATGAAATCAACCG
	R	TGCACGCGGGCATATAGTAGTAG
Pvf2	F	TCAGCGACGAAACGTGCAAGA
	R	TTTGAATGCGGCGTCGTTCC
Pvf3	F	AGCCAAATTTGTGCCGCCAAG
	R	CTGCGATGCTTACTGCTCTTCACG
upd1	F	AACTGGATCGACTATCGCAAC
	R	CTATGGCCGAGTCCTGGCTAC
upd2	F	TACAAGTTCCTGCCGAACATG
	R	ATGTGGCGGTACCAAGTCTTT
upd3	F	ACAAGTGGCGATTCTATAAGG
	R	ATGTTGCGCATGTACGTGAAG
eiger	F	GATGGTCTGGATTCCATTGC
	R	TAGTCTGCGCCAACATCATC
mnd	F	CTTTTTGGCCTTCCTGCGAC
	R	CAGCACACATATCATGGCAGC
JhI-21	F	TCTCGAGTGACAATGTGCGCTAT
	R	TGGTGGTCACTCCATTGGCA
path	F	TGTTTGATTTGCGCGGCATT
	R	TTCGACCCGCTGTCCACTAT
CG1139	F	GGAAGCAGTGGGAGTGATCC
	R	ACAAGCCCAGCACTATGGAC
CG8785	F	AGAAACGATTGGATCGGGCA
	R	ATCTGCCATCTTTTGGACCGA
CG5535	F	AAACTCGACTCCACCCTTGG
	R	GCTGGGCATTCTGTTTATTAGTGA
slif	F	TTAGAGGCCAGCTAAACCGC
	R	CCAGAGATTGGTCATGGATTTTTGA

Extended Data Table 1. List of primers used in this study.